Published for SISSA by Springer

Received: *February 9, 2015*
Revised: *May 5, 2015*
Accepted: *May 6, 2015*
Published: *June 5, 2015*

JHEP06(2015)033

Matching the Nagy-Soper parton shower at next-to-leading order

M. Czakon, H.B. Hartanto, M. Kraus and M. Worek

Institute for Theoretical Particle Physics and Cosmology, RWTH Aachen University, Otto-Blumenthal Str., D-52056 Aachen, Germany

E-mail: mczakon@physik.rwth-aachen.de, hartanto@physik.rwth-aachen.de, kraus@physik.rwth-aachen.de, worek@physik.rwth-aachen.de

Abstract: We present an Mc@Nlo-like matching of next-to-leading order QCD calculations with the Nagy-Soper parton shower. An implementation of the algorithm within the Helac-Dipoles Monte Carlo generator is used to address the uncertainties and ambiguities of the matching scheme. First results obtained using the Nagy-Soper parton shower implementation in Deductor in conjunction with the Helac-Nlo framework are given for the $pp \to t\bar{t}j + X$ process at the LHC with $\sqrt{s} = 8\,\text{TeV}$. Effects of resummation are discussed for various observables.

Keywords: Monte Carlo Simulations, NLO Computations

ArXiv ePrint: 1502.00925

doi:10.1007/JHEP06(2015)033

Contents

JHEP06(2015)033

1 Introduction

The simulation of scattering events according to field theoretical models is at the core of particle physics, as it allows for both discoveries of particles and the validation of theories. The source of practical difficulties lies primarily in the presence of strong interactions. Indeed, if the initial and/or final states involve hadrons, then non-perturbative effects will have to be included at some point. It is only due to factorization that it is possible to obtain an accurate description using perturbative methods. For some observables, the evolution of the state of the system between the high scale, where fixed order perturbation theory is adequate, and the non-perturbative scale, where it is not, requires resummation of logarithmic enhancements due to soft and collinear singularities. This can be achieved either by analytic resummation methods, or by means of parton showers. The latter are the versatile tool of choice in the communication between theory and experiment.

Parton showers have a long history [1–6]. They are based on a semi-classical picture of partons splitting into pairs of other partons. This picture corresponds to the collinear limit of QCD amplitudes in next-to-leading order (NLO) configurations. Thus, the leading singularity of collinear-soft origin may be correctly reproduced. In consequence, the approach has leading logarithmic accuracy in the most general case of many partons in the high scale process. Including pure soft effects is necessary to correctly reproduce the first subleading logarithms. Recent years have seen quite some activity in this direction [7–13]. In particular, it has been possible to include leading colour soft effects using parton showers constructed around known subtraction schemes, such as the one of Catani and Seymour [14, 15]. In a series of papers [16–25], Nagy and Soper have proposed a different concept for a parton shower. Their construction should be able to include soft effects at subleading colour. Recently, they have also provided a public code [24], Deductor, that implements a large part of their idea, albeit with the exlusion of exact colour treatment, where an extension of the leading colour approximation is used, and spin correlations.

The purpose of the present publication is to specify a matching procedure between the Nagy-Soper parton shower and a fixed order calculation at NLO. This can be achieved using at least two different ideas: Mc@Nlo [26, 27] and Powheg [28–30]. The first method, which is the one we have chosen, consists in removing double counting contributions by expanding the parton shower to first order in the strong coupling and compensating for the terms, which are already present at fixed order. This is closely related to the possibility of obtaining a subtraction scheme from the parton shower, which was exploited in refs. [31–34] for the case of the Nagy-Soper construction. In particular, the implementation within the Helac-Dipoles package [35] has proven invaluable as the basis for the present work.

Having a working tool to produce parton shower matched event samples with inclusive next-to-leading order accuracy is necessary in order to assess the differences of the new shower concept and more established alternatives. This is a second goal of our publication. Clearly, there will be differences just as there are even in analytic resummation, where a much higher logarithmic accuracy can be achieved. Nevertheless, studying particular examples allows to quantify the deviations and convince oneself that they do not point to real errors either within the concept or the implementation. For this first study we have chosen a process, which involves non-trivial colour exchange and massive partons, and

JHEP06(2015)033

requires cuts in order to even define the Born approximation cross section: top-quark pair production in association with at least one jet in hadron collisions at the Large Hadron Collider (LHC). There is one drawback of having top-quarks in the final state. A realistic description would require the inclusion of decays. We did not want to consider off-shell effects and the narrow width approximation was also out of the question for technical reasons. In such cases, one relies on the shower program to decay the quarks. This is a crude approximation, which neglects spin correlations. Unfortunately, DEDUCTOR does not even provide that. Thus, we are simulating a process with stable top-quarks in the final state. On the other hand, in our comparisons we have only taken the perturbative evolution into account. In other words, we have switched off the hadronization and multiple-interaction models available in common Monte Carlo generators (though not in DEDUCTOR). This allows us to quantify differences at the same level of approximation.

We should point out that our matching implementation is restricted to leading colour. DEDUCTOR in the version we have used contains a more advanced colour approximation. Nevertheless, as long as full colour functionality is not available, we have decided to simplify our work. On the other hand, working at leading colour is appropriate for comparisons with other systems, which are also only certified to have this accuracy.

Ours is the first phenomenological study performed using the Nagy-Soper shower, which does not involve the authors of the concept. We believe that this independence is important and actually proves that DEDUCTOR is ready to use by outsiders. It also gave us the motivation to prepare a summary of the main components of the Nagy-Soper parton shower including a list of ambiguities, which correspond to the places, where modifications might be expected once more experience in practical applications is gathered. We hope that this part of our paper will be useful to those, who do not necessarily want to read the hundreds of pages of the original publications to gain a basic understanding of the concept.

The present text is organised as follows. We start by a summary of the Nagy-Soper parton shower concept. We are explicit as far as those parts are concerned, which have an impact on the construction of the matching procedure. We also point out some special features like the modified parton distribution function (PDF) evolution for example. The next section deals with the matching itself. We consider both the case of processes, which have well-defined Born approximation total cross sections, and the case of processes, which require the specification of cuts already at this level. Subsequently, we describe the details of our implementation within HELAC-DIPOLES and the interface to DEDUCTOR. Finally, we show some results for $t\bar{t}j$ production at the LHC and compare them to results obtained with other systems. We close the main text with some short conclusions. An appendix contains a more thorough discussion of the matching in the leading colour approximation.

2 A parton shower with quantum interference

In this section we review the Nagy-Soper parton shower concept, which allows for parton state evolution to include both spin and colour correlations. Neverthless, the main focus of our discussion will lie on the colour evolution. In fact, the exponentiation of non-diagonal colour matrices is a long-standing problem. Notice that an independent attempt to include full colour evolution in a parton shower was already made in ref. [11].

JHEP06(2015)033

2.1 Quantum configuration space

A generic $2 \to m$ process is defined by two initial state partons a and b,[1] and $1, \ldots, m$ final state particles. Each particle is described by a set of quantum numbers to define the flavour f_i, spin s_i and colour c_i of the particle and its momentum p_i. Initial state partons are described by momentum fractions η_a and η_b. Thus, a complete m-parton ensemble, i.e. the probability distribution over possible quantum states, can be parametrized by the following set of quantum numbers[2]

$$\{p, f, s, c\}_m \equiv \{[\eta_a, -f_a, s_a, c_a], [\eta_b, -f_b, s_b, c_b], [p_1, f_1, s_1, c_1], \ldots, [p_m, f_m, s_m, c_m]\}\,. \quad (2.1)$$

Special emphasis should be given to initial state partons. In the Nagy-Soper shower, charm and bottom quarks are allowed to be massive. In the presence of parton masses, the initial state momenta are parametrized by the hadron momenta p_A and p_B, and the momentum fractions η_a and η_b

$$p_a = \eta_a p_A + \frac{m_{f_a}^2}{\eta_a s} p_B\,, \quad (2.2)$$

$$p_b = \eta_b p_B + \frac{m_{f_b}^2}{\eta_b s} p_A\,, \quad (2.3)$$

where $p_A^2 = p_B^2 = 0$,[3] and $s = 2(p_A \cdot p_B)$. In the following, we will describe the treatment of spin and colour in the parton shower. A matrix element $\mathcal{M}$ can be viewed as a vector $|\mathcal{M}(\{p, f\}_m)\rangle$ in colour $\otimes$ spin space and can be resolved into basis vectors $|\{s\}_m\rangle$ and $|\{c\}_m\rangle$ with complex expansion coefficients $\mathcal{M}(\{p, f, s, c\}_m)$

$$\begin{aligned} |\mathcal{M}(\{p, f\}_m)\rangle &= \sum_{\{s\}_m} \sum_{\{c\}_m} \mathcal{M}(\{p, f, s, c\}_m)\, |\{s\}_m\rangle \otimes |\{c\}_m\rangle \\ &= \sum_{\{s,c\}_m} \mathcal{M}(\{p, f, s, c\}_m)\, |\{s, c\}_m\rangle\ . \end{aligned} \quad (2.4)$$

The basis in the spin space is orthonormal. Here, $\{s\}_m = \{s_a, s_b, s_1, \ldots, s_m\}$ represents the physical helicities of all particles.

The colour basis is defined in terms of colour string configurations [36–40], which allows for a straightforward connection with a hadronization model based on colour strings like the one described in ref. [41]. In practice, a colour state $|\{c\}_m\rangle$ is represented by several strings $\{\mathcal{S}_1, \ldots, \mathcal{S}_n\}$, where $\mathcal{S}_i$ can be an open or a closed string. An open string is denoted by $\mathcal{S} = [l_1, l_2, \ldots, l_{n-1}, l_n]$, where l_1 is the label of a quark, l_n of an anti-quark and $l_2, \ldots, l_{n-1}$ are gluon labels. Furthermore, a closed string is given by $\mathcal{S} = (l_1, \ldots, l_n)$, where l_i labels only gluons this time. For brevity we will write $l_i = i$ in the following. The label l of a

[1] We treat the case of incoming hadrons. Colour neutral particles imply the usual simplifications, i.e. lack of parton distribution functions and no initial state evolution.

[2] The minus sign for the initial state flavour is only a convention, since all partons are considered as outgoing from the hard interaction.

[3] Even though parton masses are kept non-vanishing, one assumes that the proton mass is negligible with respect to the hadronic center-of-mass energy.

JHEP06(2015)033

parton refers to its colour index a_l. In case l labels a gluon, the colour index a_l has values $1,\ldots,8$. In case of quarks or anti-quarks a_l only takes the values $1,2,3$. The set of colour indices $\{a_1,a_2,\cdots,a_n\}$ is abbreviated in the following with $\{a\}$ and allows to define the colour basis structures.

The colour structure of an open string can be defined by

$$\Psi^{\{a\}}(\mathcal{S}=[1,2,\ldots,n-1,n]) = \frac{1}{\sqrt{N_c C_F^{n-2}}}[T^{a_2}T^{a_3}\cdots T^{a_{n-1}}]_{a_1 a_n}\,, \tag{2.5}$$

where T^a is an $\mathrm{SU}(N_c)$ generator. Open strings are normalized to

$$\langle\mathcal{S}|\mathcal{S}\rangle \equiv \sum_{\{a\}} |\Psi^{\{a\}}(\mathcal{S})|^2 = 1\,. \tag{2.6}$$

For closed strings we define

$$\Psi^{\{a\}}(\mathcal{S}=(1,\ldots,n)) = \frac{1}{\sqrt{C_F^n}}\mathrm{Tr}[T^{a_1}T^{a_2}\cdots T^{a_n}]\,, \tag{2.7}$$

with normalization

$$\langle\mathcal{S}|\mathcal{S}\rangle \equiv \sum_{\{a\}} |\Psi^{\{a\}}(\mathcal{S})|^2 = 1 - \left(\frac{-1}{2N_c C_F}\right)^{n-1}\,. \tag{2.8}$$

A colour state $|\{c\}_m\rangle$ is represented by a product of these colour structures. Thus a state is normalized to

$$\langle\{c\}_m|\{c\}_m\rangle = \prod_k \langle\mathcal{S}_k|\mathcal{S}_k\rangle\,. \tag{2.9}$$

With these definitions the basis is not orthonormal in general. For instance

$$\langle\{c'\}_m|\{c\}_m\rangle = \delta\left(\{c'\}_m;\{c\}_m\right) + \mathcal{O}\left(1/N_c^2\right). \tag{2.10}$$

Therefore, the basis is only orthonormal in the leading colour approximation, $N_c\to\infty$.

2.2 Quantum density matrix

The basic object describing the parton shower evolution is the quantum density matrix ρ, which gives the "probability"[4] to find a certain parton ensemble $\{p,f\}_m$. In this section we give the relation of the quantum density to matrix elements. Using the notation of the previous section, one can write the expectation value for a completely inclusive observable F, as

$$\begin{aligned}\sigma[F] &= \sum_m \frac{1}{m!}\int [d\{p,f\}_m]\,\langle\mathcal{M}(\{p,f\}_m)|\,F(\{p,f\}_m)\,|\mathcal{M}(\{p,f\}_m)\rangle\,\frac{f_a(\eta_a,\mu_F^2)f_b(\eta_b,\mu_F^2)}{4n_c(a)n_c(b)\times\text{flux}}\\ &\equiv \sum_m \frac{1}{m!}\int [d\{p,f\}_m]\,\mathrm{Tr}[\rho(\{p,f\}_m)F(\{p,f\}_m)]\,,\end{aligned} \tag{2.11}$$

[4] Since ρ contains the full colour information, it can become negative for subleading colour configurations. Thus, strictly speaking, one cannot interpret ρ as a probability distribution. Nevertheless, the standard concepts from statistical mechanics apply here.

JHEP06(2015)033

where the sum runs over all final state multiplicities. Here, $[d\{p,f\}_m]$ is the sum of all m-particle phase space measures for different flavour sequences $\{f\}_m$. The factor $1/m!$ is necessary to account for identical contributions. The parton density functions evaluated at the momentum fraction η and factorization scale μ_F^2 are denoted by $f_{a/b}(\eta,\mu_F^2)$. We average over initial state spins (factor 4 in the denominator) and colour (factor $n_c(i)$, with $n_c(q)=3$ for quarks and $n_c(g)=8$ for gluons). The trace in the second line corresponds to a sum over indices in the colour $\otimes$ spin space. The quantum density ρ is, therefore, given by

$$\begin{aligned}\rho(\{p,f\}_m) &= |\mathcal{M}(\{p,f\}_m)\rangle\,\langle\mathcal{M}(\{p,f\}_m)|\,\frac{f_a(\eta_a,\mu_F^2)f_b(\eta_b,\mu_F^2)}{4n_c(a)n_c(b)\times\text{flux}}\\ &\equiv \sum_{s,c}\sum_{s',c'}|\{s,c\}_m\rangle\,\rho(\{p,f,s',c',s,c\}_m)\,\langle\{s',c'\}_m|\,,\end{aligned} \tag{2.12}$$

where we used the expansion of $|\mathcal{M}(\{p,f\}_m)\rangle$ according to eq. (2.4). The quantum density matrix is a projector onto the different helicity and gauge invariant subamplitudes of the full quantum amplitude

$$\rho(\{p,f,s',c',s,c\}_m) = \mathcal{M}^*(\{p,f,s',c'\}_m)\mathcal{M}(\{p,f,s,c\}_m)\frac{f_a(\eta_a,\mu_F^2)f_b(\eta_b,\mu_F^2)}{4n_c(a)n_c(b)\times\text{flux}}\,. \tag{2.13}$$

Using the quantum density matrix, the expectation value of the observable F is given by[5]

$$\sigma[F] = \sum_m \frac{1}{m!}\int [d\{p,f,s',c',s,c\}_m]F(\{p,f\}_m)\,\langle\{s',c'\}_m|\{s,c\}_m\rangle\,\rho(\{p,f,s',c',s,c\}_m)\,, \tag{2.14}$$

where the integration measure has been extended by the inclusion of the summation over spin and colour. It is useful to define basis vectors or statistical states $|\{p,f,s',c',s,c\}_m)$ (see ref. [16]), such that

$$\rho(\{p,f,s',c',s,c\}_m) = (\{p,f,s',c',s,c\}_m|\rho)\,. \tag{2.15}$$

Defining additionally an abstract state $(F|$ according to

$$(F|\{p,f,s',c',s,c\}_m) = F(\{p,f\}_m)\,\langle\{s',c'\}_m|\{s,c\}_m\rangle \tag{2.16}$$

and using the decomposition of the identity

$$1 = \sum_m \frac{1}{m!}\int [d(\{p,f,s',c',s,c\}_m)]|\{p,f,s',c',s,c\}_m)(\{p,f,s',c',s,c\}_m|\,, \tag{2.17}$$

one can reduce eq. (2.14) to a scalar product

$$\sigma[F] = (F|\rho)\,. \tag{2.18}$$

Finally, we define the total cross section measurement function $(1|$ as

$$(1|\{p,f,s',c',s,c\}_m) = \langle\{s'\}_m|\{s\}_m\rangle\,\langle\{c'\}_m|\{c\}_m\rangle\,. \tag{2.19}$$

[5]We assume that F is a unit operator in colour $\otimes$ spin space.

JHEP06(2015)033

2.3 Evolution equation

The evolution equation describes the propagation of the quantum density matrix ρ from some initial shower time t_0 to some final time t_F. The initial time corresponds to the hard interaction, while the final to the formation of hadrons. Therefore, t_F characterizes the physical scale at which parton emissions cannot be described perturbatively. There is no unique definition of shower time t as explained in more detail in the upcoming section 2.7.

The perturbative evolution is described by an operator $\mathrm{U}(t_F, t_0)$. The expectation value of the observable F, including shower effects, is

$$\sigma[F] = (F|\rho(t_F)) = (F|\mathrm{U}(t_F, t_0)|\rho(t_0))\,. \tag{2.20}$$

$\mathrm{U}(t_F, t_0)$ is assumed to be unitary[6] in the sense that the total cross section σ_T is not affected by evolution

$$\sigma_T = (1|\rho(t_F)) = (1|\mathrm{U}(t_F, t_0)|\rho(t_0)) = (1|\rho(t_0))\,. \tag{2.21}$$

The evolution operator is the solution of the equation

$$\frac{d\mathrm{U}(t, t_0)}{dt} = [\mathcal{H}_I(t) - \mathcal{V}(t)]\mathrm{U}(t, t_0)\,. \tag{2.22}$$

Here, $\mathcal{H}_I(t)$ describes the transformation of a state $\{p, f, s', c', s, c\}_m$ to another state $\{\hat{p}, \hat{f}, \hat{s}', \hat{c}', \hat{s}, \hat{c}\}_{m+1}$ by the emission of a resolved particle. This transition between the states is of course constrained by overall momentum conservation. On the other hand, $\mathcal{V}(t)$ describes the unresolved/virtual emission and, therefore, does not alter momentum or flavour configurations of the particles. Nevertheless, it can change colour configurations, which can have an effect on further emissions. It can be further decomposed into a colour diagonal, $\mathcal{V}_E(t)$, and a colour off-diagonal part, $\mathcal{V}_S(t)$

$$\mathcal{V}(t) = \mathcal{V}_E(t) + \mathcal{V}_S(t)\,. \tag{2.23}$$

Traditional parton showers correspond to the large N_c limit. The colour structure is, therefore, always diagonal ($\mathcal{V}_S(t) \to 0$). In that case, eq. (2.22) can be solved as

$$\mathrm{U}(t, t_0) = N(t, t_0) + \int_{t_0}^{t} d\tau\ \mathrm{U}(t, \tau)\mathcal{H}_I(\tau)N(\tau, t_0)\,, \tag{2.24}$$

where $N(t, t_0)$ is the Sudakov form factor (a number) defined as

$$N(t, t_0) = \exp\left(-\int_{t_0}^{t} d\tau\ \mathcal{V}(\tau)\right)\,. \tag{2.25}$$

In case of a non-trivial colour evolution, the exponentiation of a non-diagonal matrix is cumbersome. Instead, only the colour diagonal part, $\mathcal{V}_E(t)$, is exponentiated while the off-diagonal part, $\mathcal{V}_S(t)$ is treated perturbatively on the same footing as $\mathcal{H}_I(t)$

$$\mathrm{U}(t, t_0) = N(t, t_0) + \int_{t_0}^{t} d\tau\ \mathrm{U}(t, \tau)\left[\mathcal{H}_I(\tau) - \mathcal{V}_S(\tau)\right] N(\tau, t_0)\,, \tag{2.26}$$

[6] A non-unitary evolution can be used to resum soft gluon effects.

JHEP06(2015)033

with

$$N(t,t_0) = \exp\left(-\int_{t_0}^{t} d\tau\ \mathcal{V}_E(\tau)\right). \tag{2.27}$$

This is the final evolution equation of the Nagy-Soper parton shower. Notice, however, that the current implementation in DEDUCTOR involves some approximations which are documented in section 2.6.

In the following we provide the definitions of the real splitting operator $\mathcal{H}_I(t)$ and the virtual operator $\mathcal{V}(t)$. As we will see, the unitarity condition on $\mathrm{U}(t,t_F)$ will allow to determine $\mathcal{V}(t)$ in terms of $\mathcal{H}_I(t)$.

2.4 $\mathcal{H}_I(t)$ — real splitting operator

The real splitting operator describes the transition of an m-particle ensemble to an $(m+1)$-particle one, by splitting a particle into two,

$$\{p,f,s',c',s,c\}_m \to \{\hat{p},\hat{f},\hat{s}',\hat{c}',\hat{s},\hat{c}\}_{m+1}\,. \tag{2.28}$$

This splitting is constrained by flavour and momentum conservation. The parameters of the transition require further specifications, because they depend on a particular choice of momentum mappings, shower time and splitting functions. The behaviour of the splitting operator is fixed in the infrared regime in order to reproduce the correct singular limits of QCD amplitudes.

After emitting a particle, one has to modify the momenta in the event to preserve momentum conservation and the on-shellness of all particles. This is achieved by momentum mappings R_l, which require three additional variables parametrizing the momentum of the emitted particle, Γ_l, and a variable, χ_l, specifying its flavour $\hat{f}_{m+1}$. Thus, the new momenta and flavours are given by

$$\{\hat{p},\hat{f}\}_{m+1} = R_l(\{p,f\}_m,\Gamma_l,\chi_l)\,, \tag{2.29}$$

where $l \in \{a,b,1,\ldots,m\}$. The inverse of this transformation is denoted by Q_l

$$Q_l(\{\hat{p},\hat{f}\}_{m+1}) = \{p,f\}_m\,. \tag{2.30}$$

The Nagy-Soper parton shower makes use of a global momentum mapping [16], i.e. all final state particles' momenta are modified to account for the momentum of the emitted particle. The freedom inherent in the definition of R_l may be exploited to improve the resummation for certain observables. For instance, the study presented in ref. [19] has shown, that the p_T spectrum for Drell-Yan Z-boson production depends strongly on the momentum mapping for initial state parton splittings. The original R_l from ref. [16] has been found inadequate and subsequently modified in ref. [22]. The modified version has been adopted in DEDUCTOR.

One can define a momentum mapping operator $\mathcal{P}_l$ satisfying two conditions, the first one being

$$\frac{1}{m!}\int [d\{p',f'\}_m]\,(\{\hat{p},\hat{f}\}_{m+1}|\mathcal{P}_l|\{p',f'\}_m)\,g(\{p',f'\}_m) = g(\{p,f\}_m)\,, \tag{2.31}$$

where $g(\{p,f\}_\lambda)$ is an arbitrary test function and $\{p,f\}_m$ is determined by eq. (2.30). The second condition is

$$\frac{1}{(m+1)!}\int [d\{\hat{p},\hat{f}\}_{m+1}]\, g(\{\hat{p},\hat{f}\}_{m+1})\,(\{\hat{p},\hat{f}\}_{m+1}|\mathcal{P}_l|\{p,f\}_m) \\ = \frac{1}{(m+1)}\sum_{\hat{f}_{m+1}\in\chi_l}\int d\Gamma_l\, g(\{\hat{p}',\hat{f}'\}_{m+1})\,, \tag{2.32}$$

where $\{\hat{p}',\hat{f}'\}_{m+1}$ is determined by eq. (2.29). $\mathcal{P}_l$ contains a δ-function, which links the $(m+1)$-particle kinematics to the m-particle kinematics with R_l. The two conditions imply that the Jacobians resulting from the integration over the δ-function in eqs. (2.31) and (2.32) have been absorbed in $\mathcal{P}_l$.

The evolution of the density matrix can be determined by studying the factorization of QCD amplitudes in the soft and collinear limits. We remind that in the limit when two partons become collinear, $\hat{p}_l \parallel \hat{p}_{m+1}$, the amplitude factorizes as

$$|\mathcal{M}(\{\hat{p},\hat{f}\}_{m+1})\rangle \approx T_l^\dagger(f_l \to \hat{f}_l + \hat{f}_{m+1}) V_l^\dagger(\{\hat{p},\hat{f}\}_{m+1})\,|\mathcal{M}(\{p,f\}_m)\rangle\,, \tag{2.33}$$

where $T_l^\dagger(f_l \to \hat{f}_l + \hat{f}_{m+1})$ is an operator in colour space (see ref. [16]). $V_l^\dagger(\{\hat{p},\hat{f}\}_{m+1})$ is the splitting operator in spin space. Contrary to traditional parton showers, the Nagy-Soper formulation does not use the Altarelli-Parisi splitting kernels [42]. Instead, the required functions are derived directly from matrix elements without taking the collinear limit first [16]. This allows, for example, for a direct access to polarization information. Furthermore, the functions are not singular in the soft limit [17]. In the soft limit, on the other hand, when the momentum of a gluon $\hat{p}_{m+1}$ vanishes, a similar approximation is valid

$$|\mathcal{M}(\{\hat{p},\hat{f}\}_{m+1})\rangle \approx \sum_l T_l^\dagger(f_l \to \hat{f}_l + \hat{f}_{m+1}) V_l^{\mathrm{soft}\,\dagger}(\{\hat{p},\hat{f}\}_{m+1})\,|\mathcal{M}(\{p,f\}_m)\rangle\,, \tag{2.34}$$

where l runs over all partons and V_l^{soft} is an eikonal factor.

Combining these approximations, we may write the following evolution equation for the quantum density matrix

$$|\rho_{m+1}) = \sum_l \mathcal{S}_l\,|\rho_m)\,. \tag{2.35}$$

Consequently $\mathcal{H}_I(t)$ is defined by the splitting operators $\mathcal{S}_l$ at a fixed shower time $\mathcal{T}_l(\{p,f\}_m)$ (see section 2.7)

$$\mathcal{H}_I(t) = \sum_l \mathcal{S}_l\,\delta\big(t - \mathcal{T}_l(\{p,f\}_m)\big)\,. \tag{2.36}$$

We shall not reproduce the exact form of $\mathcal{S}_l$ in the most general case, as it can be found in ref. [16]. Nevertheless, we would like to point out that there is an ambiguity in distributing the soft limit among the contributions with different momentum mappings. In order to illustrate this issue, we give the form of $\mathcal{H}_I(t)$ in the slightly less involved spin

JHEP06(2015)033

averaged case

$$
\begin{aligned}
&\Big(\{\hat{p},\hat{f},\hat{c}',\hat{c}\}_{m+1}|\mathcal{H}_I(t)|\{p,f,c',c\}_m\Big)\\
&\quad=(m+1)\sum_{l,k}\delta\big(t-\mathcal{T}_l(\{p,f\}_m)\big)\,(\{\hat{p},\hat{f}\}_{m+1}|\mathcal{P}_l|\{p,f\}_m)\\
&\qquad\times\frac{n_c(a)n_c(b)\eta_a\eta_b}{n_c(\hat{a})n_c(\hat{b})\hat{\eta}_a\hat{\eta}_b}\frac{f_{\hat{a}/A}(\hat{\eta}_a,\mu_F^2)f_{\hat{b}/B}(\hat{\eta}_b,\mu_F^2)}{f_{a/A}(\eta_a,\mu_F^2)f_{b/B}(\eta_b,\mu_F^2)}\\
&\qquad\times\frac{1}{2}\Big[\delta_{kl}\big(1-\delta_{\hat{f}_{m+1},g}\big)\overline{w}_{ll}(\{\hat{p},\hat{f}\}_{m+1})\\
&\qquad+\delta_{kl}\delta_{\hat{f}_{m+1},g}\Big[\overline{w}_{ll}(\{\hat{p},\hat{f}\}_{m+1})-\overline{w}_{ll}^{\text{eikonal}}(\{\hat{p},\hat{f}\}_{m+1})\Big]\\
&\qquad-(1-\delta_{kl})\delta_{\hat{f}_{m+1},g}A_{lk}(\{\hat{p}\}_{m+1})\overline{w}_{lk}^{\text{dipole}}(\{\hat{p},\hat{f}\}_{m+1})\Big]\\
&\qquad\times\Big[(\{\hat{c}',\hat{c}\}_{m+1}|T_l^\dagger(f_l\to\hat{f}_l+\hat{f}_{m+1})\otimes T_k(f_k\to\hat{f}_k+\hat{f}_{m+1})|\{c',c\}_m)\\
&\qquad\quad+(\{\hat{c}',\hat{c}\}_{m+1}|T_k^\dagger(f_k\to\hat{f}_k+\hat{f}_{m+1})\otimes T_l(f_l\to\hat{f}_l+\hat{f}_{m+1})|\{c',c\}_m)\Big]\,,
\end{aligned}
\tag{2.37}
$$

where the sum runs over two partons l and k, not necessarily different, and l is the emitter. The function $\overline{w}_{ll}$ is the spin averaged squared splitting function, while $\overline{w}_{ll}^{\text{eikonal}}$ is its soft approximation (see refs. [17, 21]). Furthermore,

$$
\overline{w}_{lk}^{\text{dipole}}(\{\hat{p},\hat{f}\}_{m+1})=-4\pi\alpha_s\frac{((\hat{p}_{m+1}\cdot\hat{p}_l)\hat{p}_k-(\hat{p}_{m+1}\cdot\hat{p}_k)\hat{p}_l)^2}{(\hat{p}_{m+1}\cdot\hat{p}_l)^2(\hat{p}_{m+1}\cdot\hat{p}_k)^2}\,,
\tag{2.38}
$$

which, for massless l and k, reduces to the well known squared eikonal factor [43]. The function $A_{lk}(\{\hat{p}\}_{m+1})$ removes the singularity when the partons $m+1$ and k become collinear.

$$
A_{lk}(\{\hat{p}\}_{m+1})=\frac{(\hat{p}_{m+1}\cdot\hat{p}_k)(\hat{p}_l\cdot\hat{Q})}{(\hat{p}_{m+1}\cdot\hat{p}_k)(\hat{p}_l\cdot\hat{Q})+(\hat{p}_{m+1}\cdot\hat{p}_l)(\hat{p}_k\cdot\hat{Q})}\,,
\tag{2.39}
$$

where $\hat{Q}$ is the total final state momentum. The ambiguity we have mentioned is due to the fact that the product $A_{lk}\,\overline{w}_{lk}^{\text{dipole}}$ must only satisfy two conditions: 1) it may not have a singularity in the collinear limit $\hat{p}_{m+1}\parallel\hat{p}_k$; 2) it should correctly reproduce the singularity at $\hat{p}_{m+1}\to 0$. Formulae (2.38) and (2.39) only correspond to one specific choice.

2.5 $\mathcal{V}(t)$ — virtual splitting operator

As advertised, the virtual splitting operator, $\mathcal{V}(t)$, can be determined to a large extent from the real splitting operator $\mathcal{H}_I(t)$ by the requirement of unitarity

$$
\big(1\big|\mathcal{H}_I(t)-\mathcal{V}(t)\big|\rho(t)\big)=0\,,
\tag{2.40}
$$

which should be valid for any $|\rho(t))$. This can be interpreted with the help of the optical theorem. For example, we can schematically write

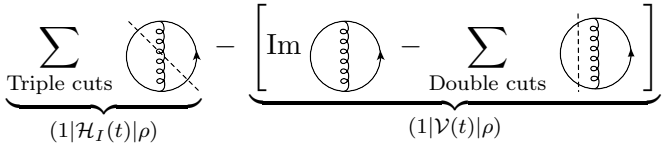

$$
=0\,.
\tag{2.41}
$$

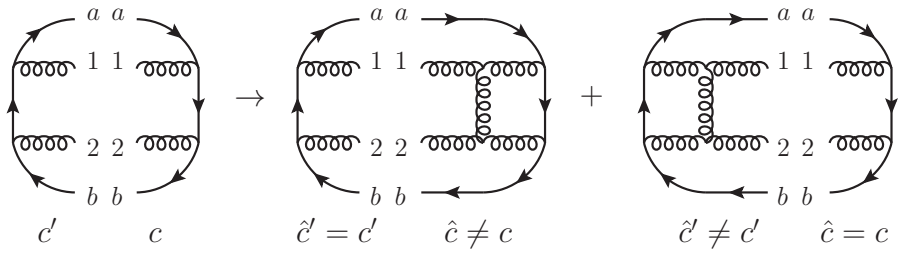

Figure 1. Modification on the colour structure by the inclusion of the virtual operator $\mathcal{V}(t)$.

Notice that $\mathcal{V}(t)$ does not contain the exact virtual corrections. Furthermore, it turns out that $(1|\mathcal{H}_I(t)|\{p,f,s',c',s,c\}_m)$ does not contain spin correlations due to the integration over the azimuthal angle of the emitted partons [16]. This allows us to write

$$(1|\mathcal{H}_I(t)|\{p,f,s',c',s,c\}_m) \equiv 2\,\langle\{s'\}_m|\{s\}_m\rangle\,\langle\{c'\}_m|h(t,\{p,f\}_m)|\{c\}_m\rangle\ . \tag{2.42}$$

In consequence, the freedom in defining $\mathcal{V}(t)$ is restricted to the colour structure. In principle, a virtual correction may be applied either on the c' or c indices of the $|\{c',c\}_m)$ state, see figure 1. This leads to the following

$$\mathcal{V}(t) = (h + i\phi)\otimes 1 + 1\otimes(h^\dagger - i\phi)\,, \tag{2.43}$$

where ϕ is a colour dependent phase, which can not be determined from real radiation corrections. Its presence is a consequence of a Coulomb gluon exchange [21]

$$\phi(t,\{p,f\}_m) = -2\pi\sum_{l\neq k}\frac{\alpha_s}{4\pi}\frac{1}{v_{kl}}\mathbf{T}_k\cdot\mathbf{T}_l\,, \qquad v_{kl} = \sqrt{1-\frac{m_{f_k}^2 m_{f_l}^2}{(p_k\cdot p_l)^2}}\,, \tag{2.44}$$

where the sum runs over l and k, both either in the initial or final state. Examples of the relationship between $\mathcal{H}_I(t)$ and $\mathcal{V}(t)$ are depicted in figure 2. The exact specification of $\mathcal{V}(t)$ can be found in refs. [16, 21].

2.6 Colour and spin evolution

An essential part of the action of $\mathcal{H}_I(t)$ is the change of the colour state. Starting from the two types of colour strings eqs. (2.5) and (2.7), the application of $T_l^\dagger(f_l\to\hat{f}_l+\hat{f}_{m+1})$ on the c' index and of $T_k(f_k\to\hat{f}_k+\hat{f}_{m+1})$ on the c index of the $|\{c',c\}_m)$ state results in a linear combination of the same basis vectors. This follows from the relations

$$if^{abc}T^c = [T^a,T^b] = T^aT^b - T^bT^a\,, \tag{2.45}$$

$$T^a_{ij}T^a_{kl} = \frac{1}{2}\left[\delta_{il}\delta_{jk} - \frac{1}{N_c}\delta_{ij}\delta_{kl}\right]\,, \tag{2.46}$$

which can be translated into similar relations for $T^{(\dagger)}(f_l\to\hat{f}_l+\hat{f}_{m+1})$, see ref. [16].

In principle we have to consider diagonal, $\{c'\}_m=\{c\}_m$, and off-diagonal, $\{c'\}_m\neq\{c\}_m$, colour configurations, see figure 3 for illustration. Notice that the colour diagonal

JHEP06(2015)033

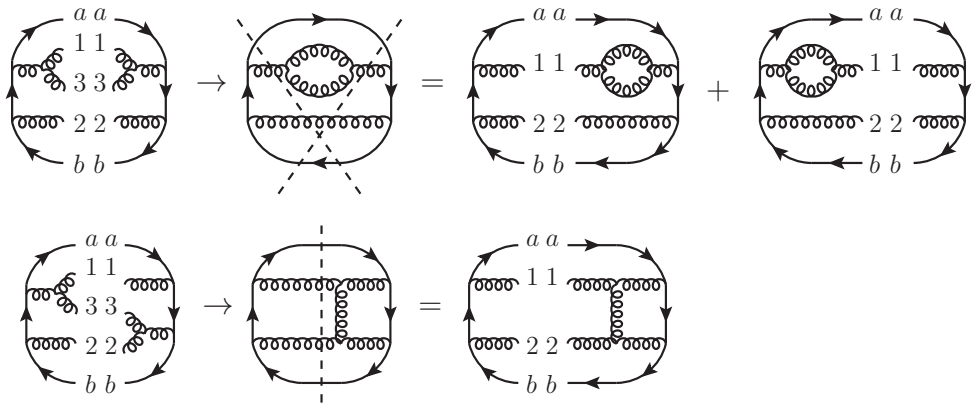

Figure 2. Correspondence between a real radiation contribution as given by $\mathcal{H}_I(t)$ and its counterpart in $\mathcal{V}(t)$, for a direct splitting (upper line) and an interference contribution (lower line). In both cases the left part of the first graph corresponds to $l = 1$. For the right part $k = 1$ (upper graph) or $k = 2$ (lower graph). In the case of the interference contribution, by convention, we attach the virtual correction to the amplitude of the parton k.

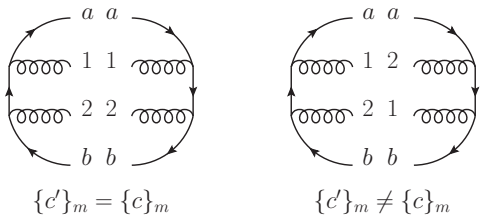

Figure 3. Example colour configurations for the $\bar{q}(a)q(b)g(1)g(2)$ state.

contributions contain the leading colour contribution, while colour off-diagonal contributions are subleading. The latter can be identified by crossing of gluon lines. Traditional parton showers are restricted to the leading colour approximation (or at best to colour diagonal contributions). On the other hand, the Nagy-Soper parton shower allows for the evolution of subleading colour configurations. In figures 4, 5, 6, 7, and 8, we give several examples of colour evolution induced by direct splitting (application of $T_l^\dagger \otimes T_l$) and interference contributions (application of $T_l^\dagger \otimes T_k$, where $l \neq k$).

The solution of the evolution equation, eq. (2.26), requires a decomposition of the virtual operator into a diagonal and an off-diagonal colour part. This can be achieved with the help of the LC+ approximation introduced in ref. [21]. The main features of this approximation are

1. Exact colour treatment of the collinear and soft-collinear limits;

2. Leading colour approximation for the pure soft limit (a part of the subleading contributions is kept nevertheless).

According to the previous section, the virtual splitting operator is defined in terms of the real splitting operator. For the latter, the LC+ approximation amounts to the

JHEP06(2015)033

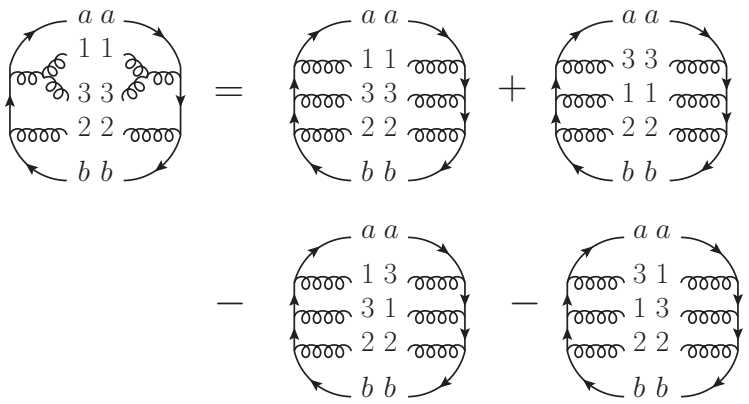

Figure 4. Example of a direct splitting $g \to gg$ starting from a diagonal colour configuration. The left part of the first graph corresponds to $l = 1$, while the right part to $k = 1$. Moreover, $m+1 = 3$.

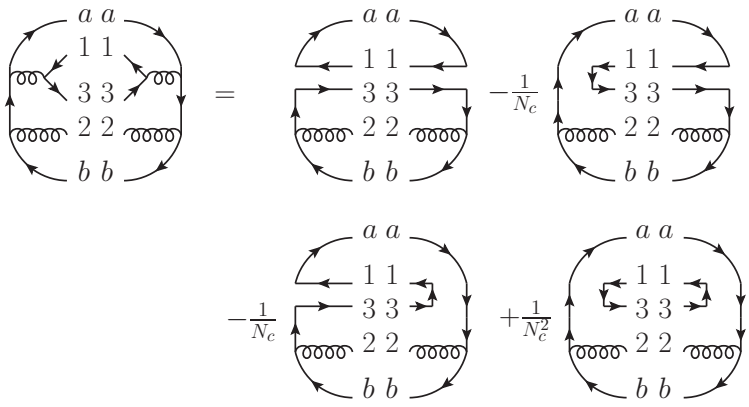

Figure 5. Example of a direct splitting $g \to q\bar{q}$ starting from a diagonal colour configuration. The left part of the first graph corresponds to $l = 1$, while the right part to $k = 1$. Moreover, $m+1 = 3$.

introduction of a projector $C(l, m+1)$ acting on the colour states $|\{c\}_{m+1}\rangle$ in eq. (2.37) as

$$T_k^\dagger(f_k \to \hat{f}_k + \hat{f}_{m+1})\,|\{c\}_m\rangle \to C(l, m+1) T_k^\dagger(f_k \to \hat{f}_k + \hat{f}_{m+1})\,|\{c\}_m\rangle\,, \tag{2.47}$$

$$\langle\{c'\}_m|\,T_k(f_k \to \hat{f}_k + \hat{f}_{m+1}) \to \langle\{c'\}_m|\,T_k(f_k \to \hat{f}_k + \hat{f}_{m+1}) C^\dagger(l, m+1)\,, \tag{2.48}$$

where

$$C(l, m+1)\,|\{c\}_{m+1}\rangle = \begin{cases} |\{c\}_{m+1}\rangle & \text{partons } l \text{ and } m+1 \text{ form a } q\bar{q} \text{ pair}\,, \\ |\{c\}_{m+1}\rangle & \text{partons } l \text{ and } m+1 \text{ are colour connected}\,, \\ 0 & \text{otherwise}\,. \end{cases} \tag{2.49}$$

Colour connected partons are partons, which are direct neighbours on a colour string as defined in section 2.1. The definition eq. (2.49) guarantees that direct splittings are treated exactly. This is also true for the evolution of off-diagonal colour configurations, as depicted in figure 6. In other cases, a part of the contributions is removed, as can be seen in figures 7 and 8.

JHEP06(2015)033

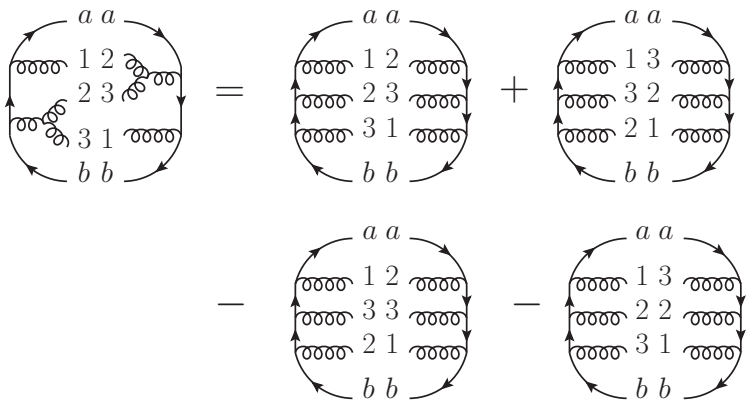

Figure 6. Example of a direct splitting $g \to gg$ starting from an off-diagonal colour configuration. The left part of the first graph corresponds to $l = 2$, while the right part to $k = 2$. Moreover, $m + 1 = 3$.

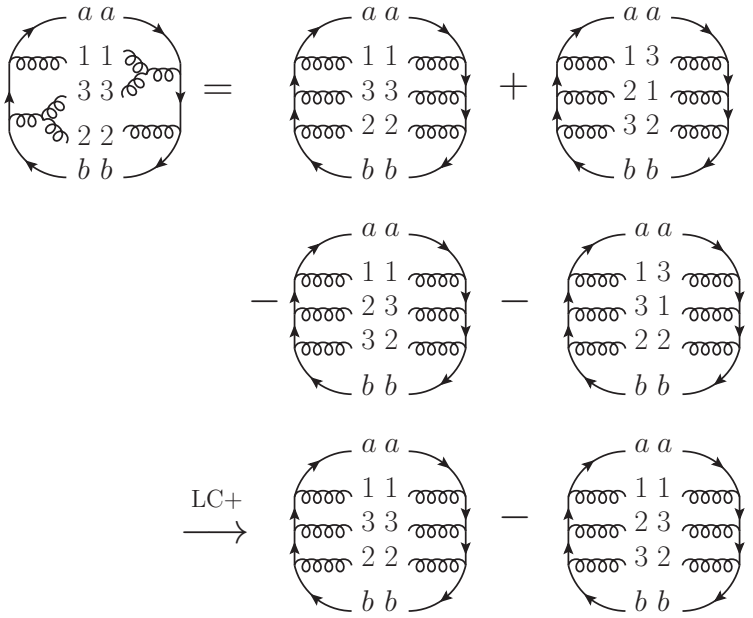

Figure 7. Example of an interference contribution of two $g \to gg$ splittings starting from a diagonal colour configuration. The last line represents the LC+ approximation of the original colour structure. The left part of the first graph corresponds to $l = 2$, while the right part to $k = 1$. Moreover, $m + 1 = 3$.

The colour projector $C(l, m+1)$ defines a decomposition

$$\mathcal{H}_I(t) \equiv \mathcal{H}_I^{\mathrm{LC+}}(t) + \Delta\mathcal{H}_I(t)\,. \tag{2.50}$$

All corrections to the LC+ approximation are of order $\mathcal{O}(1/N_c^2)$ and are treated perturbatively. It turns out that the virtual splitting operator $\mathcal{V}^{\mathrm{LC+}}(t)$ defined in terms of $\mathcal{H}_I^{\mathrm{LC+}}(t)$ is colour diagonal [21]. Therefore, we define

$$\mathcal{V}_E(t) \equiv \mathcal{V}^{\mathrm{LC+}}(t)\,, \qquad \mathcal{V}_S(t) \equiv \Delta\mathcal{V}(t) = \mathcal{V}(t) - \mathcal{V}^{\mathrm{LC+}}(t)\,. \tag{2.51}$$

JHEP06(2015)033

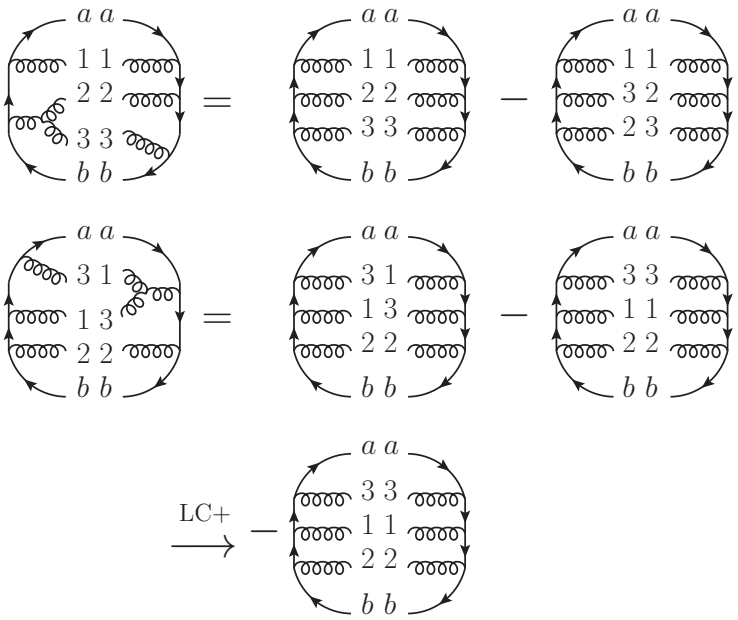

Figure 8. Example of interference contributions of $g \to gg$ and $q \to qg$ splittings starting from a diagonal colour configuration. Upper graph: the left part of the first graph corresponds to $l = 2$, while the right part to $k = b$. Lower graph: the left part of the first graph corresponds to $l = a$, while the right part to $k = 1$. Moreover, $m + 1 = 3$ in both cases. The last line represents the LC+ approximation of the original colour structure of the lower graph.

We can also define an approximate evolution operator

$$U^{\mathrm{LC+}}(t, t_0) = N^{\mathrm{LC+}}(t, t_0) + \int_{t_0}^{t} d\tau \; U^{\mathrm{LC+}}(t, \tau) \mathcal{H}_I^{\mathrm{LC+}}(\tau) N^{\mathrm{LC+}}(\tau, t_0) \,, \tag{2.52}$$

where

$$N^{\mathrm{LC+}}(t, t_0) = \exp\left(- \int_{t_0}^{t} d\tau \; \mathcal{V}^{\mathrm{LC+}}(\tau) \right) . \tag{2.53}$$

On the other hand, the exact evolution operator is

$$\mathrm{U}(t, t_0) = U^{\mathrm{LC+}}(t, t_0) + \int_{t_0}^{t} d\tau \; \mathrm{U}(t, \tau) \left[\Delta\mathcal{H}_I(\tau) - \Delta\mathcal{V}(\tau) \right] U^{\mathrm{LC+}}(\tau, t_0) \,. \tag{2.54}$$

The practical solution of these equations is described in ref. [21]. The current implementation of DEDUCTOR relies on eq. (2.52).

Let us comment on the logarithmic accuracy of the Nagy-Soper parton shower. Consider an observable $\mathcal{O}$, given by the expansion

$$\langle \mathcal{O} \rangle = \sum_n c(n, 2n) \alpha_s^n L^{2n} + \sum_n c(n, 2n-1) \alpha_s^n L^{2n-1} + \cdots \,, \tag{2.55}$$

where L denotes a potentially large logarithm, e.g. $L = \log(s/p_T^2)$, where s is the scale of the hard process, and p_T is the transverse momentum of some final state, for example

JHEP06(2015)033

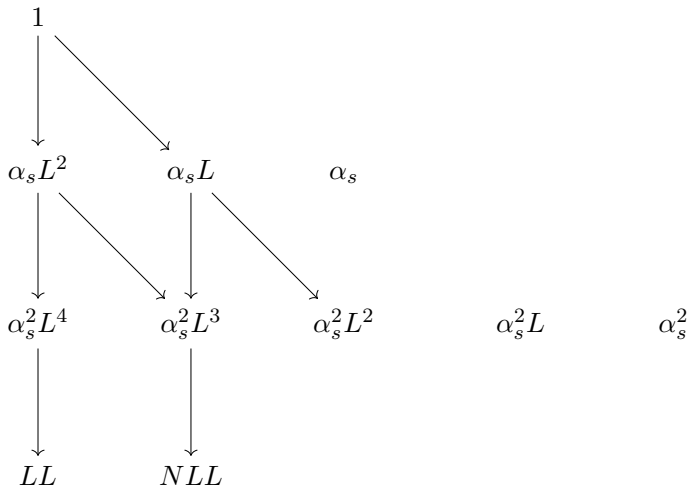

Figure 9. Illustration of the logarithm counting. One step in the vertical direction is given by an insertion of $U^{\mathrm{LC+}}$ and a diagonal step is given by an insertion of $\Delta\mathcal{H}_I(t) - \Delta\mathcal{V}(t)$. One can see, that two insertions of $\Delta\mathcal{H}_I(t) - \Delta\mathcal{V}(t)$ only contributes to the coefficient of $\alpha_s^n L^{2n-2}$.

a pair of oppositely charged leptons from the Drell-Yan process. The evolution operator $\mathrm{U}(t, t_0)$ reproduces the coefficients $c(n, 2n)$ and $c(n, 2n-1)$ without any approximations in colour. On the other hand, $U^{\mathrm{LC+}}(t, t_0)$ misses part of the $c(n, 2n-1)$ coefficient due to subleading colour contributions from wide angle soft radiation. For this reason, the LC+ approximation is only exact at leading logarithm (LL), see figure 9. Inserting a factor of $[\Delta\mathcal{H}_I(\tau) - \Delta\mathcal{V}(\tau)]$ generates the remaining contribution to the coefficient $c(n, 2n-1)$. In consequence, the evolution operator

$$\mathrm{U}(t, t_0) = U^{\mathrm{LC+}}(t, t_0) + \int_{t_0}^{t} d\tau\; U^{\mathrm{LC+}}(t, \tau)\,[\Delta\mathcal{H}_I(\tau) - \Delta\mathcal{V}(\tau)]\,U^{\mathrm{LC+}}(\tau, t_0)\,, \tag{2.56}$$

is accurate at next-to-leading logarithm (NLL).

As pointed out before (see discussion around eq. (2.42)), the virtual splitting operator is diagonal in spin. Therefore, spin dependent effects are only induced by the action of $\mathcal{H}_I(t)$. It has been proposed in ref. [18] to include them on top of the spin averaged shower. To this end, we note that the necessary modification in $\mathcal{H}_I(t)$, eq. (2.37), amounts to the replacement

$$\Phi_{lk}(\{\hat{p}, \hat{f}\}_{m+1}) \;\longrightarrow\; (\{\hat{s}', \hat{s}\}_{m+1}|Y_{lk}(\{\hat{p}, \hat{f}\}_{m+1})|\{s', s\}_m)\;\Phi_{lk}(\{\hat{p}, \hat{f}\}_{m+1})\,, \tag{2.57}$$

where

$$\begin{aligned}\Phi_{lk}(\{\hat{p}, \hat{f}\}_{m+1}) = {}& \delta_{kl}\,\left(1 - \delta_{\hat{f}_{m+1},g}\right)\,\overline{w}_{ll}(\{\hat{p}, \hat{f}\}_{m+1} \\ & + \delta_{kl}\,\delta_{\hat{f}_{m+1},g}\,\left[\overline{w}_{ll}(\{\hat{p}, \hat{f}\}_{m+1} - \overline{w}_{ll}^{\mathrm{eikonal}}\right] \\ & - (1 - \delta_{kl})\,\delta_{\hat{f}_{m+1},g}\,A_{lk}(\{\hat{p}_{m+1}\})\,\overline{w}_{lk}^{\mathrm{dipole}}(\{\hat{p}, \hat{f}\}_{m+1})\,,\end{aligned} \tag{2.58}$$

and $Y_{lk}(\{\hat{p}, \hat{f}\}_{m+1})$ is just the ratio between spin dependent and spin averaged splitting functions, see ref. [18].

JHEP06(2015)033

The parton shower evolution starts with a quantum density matrix

$$(\{p, f, s', c', s, c\}_m|\rho(t_0)) = (\{p, f, c', c\}_m|\rho(t_0)) \otimes (\{s', s\}_m|\rho^s(\{p, f, c', c\}_m)) \,, \tag{2.59}$$

with a factorized spin dependence, $|\rho^s)$, with respect to the spin averaged quantum density $|\rho(t_0))$. The latter subsequently undergoes spin averaged evolution. On the other hand, after $(n-m)$ real emission steps

$$|\rho^s_n) = Y_{l_n,k_n}(\{\hat{p}, \hat{f}\}_n) \cdots Y_{l_{m+2},k_{m+2}}(\{\hat{p}, \hat{f}\}_{m+2}) Y_{l_{m+1},k_{m+1}}(\{\hat{p}, \hat{f}\}_{m+1})|\rho^s(\{p, f, c', c\}_m)) \,. \tag{2.60}$$

Assuming that the final observable does not depend on the spin configuration, we obtain

$$\sigma[F] = \sum_\lambda \frac{1}{\lambda!} \int [d\{p, f, c', c\}_\lambda](F|\{p, f, c', c\}_\lambda)(\{p, f, c', c\}_\lambda|\rho(t_F))(1_{\text{spin}}|\rho^s_\lambda) \,, \tag{2.61}$$

where

$$(1_{\text{spin}}|\rho^s_\lambda) = \sum_{\{s',s\}_\lambda} (1_{\text{spin}}|\{s', s\}_\lambda)(\{s', s\}_\lambda|\rho^s_\lambda) = \sum_{\{s\}_\lambda} (\{s, s\}_\lambda|\rho^s_\lambda) \,. \tag{2.62}$$

2.7 Shower time

The forward evolution in the shower time is used to enforce an ordering in some chosen kinematic variable. This is necessary in order to correctly resum leading logarithms of infrared sensitive quantities. In traditional parton shower programs the following ordering variables are used:

virtuality: the invariant mass of two daughter partons produced through the splitting (e.g. Pythia6Q [44]),

transverse momentum: the transverse momentum of the daughter partons with respect to the mother parton (e.g. Pythia8 [45]),

angle: the angle between the momenta of the daughter partons (e.g. Herwig [46, 47]).

The construction of a new parton shower allows to re-evaluate the advantages of these variables, and replace them if necessary. In ref. [22], the following variable has been proposed

$$\Lambda_l^2 = \frac{|(\hat{p}_l \pm \hat{p}_{m+1})^2 - m_l^2|}{2p_l \cdot Q_0} Q_0^2 \,, \tag{2.63}$$

where $\hat{p}_l$ is the emitter momentum after emission (daughter parton), $\hat{p}_{m+1}$ the emitted parton momentum (daughter parton), p_l the emitter momentum before emission (mother parton with mass m_l) and Q_0 is the total final state momentum. The minus sign between $\hat{p}_l$ and $\hat{p}_{m+1}$ in eq. (2.63) applies to an initial state splitting. The shower time with Λ_l^2 ordering is then given by

$$\mathcal{T}_l(\{p, f\}_m) \equiv -\log\left(\frac{\Lambda_l^2}{Q_0^2}\right) \,. \tag{2.64}$$

The particular form of Λ_l^2 may be justified as follows [22]. Consider a splitting of a final state parton with momentum p_0 into two partons with momenta p_1 and p_2. After splitting the mother parton has non-vanishing additional virtuality v_0^2 $(= p_0^2 - m_0^2)$, while both daughter partons are on-shell. In subsequent steps, both daughter partons will split as well, and acquire additional virtualities v_1^2 and v_2^2 $(= p_i^2 - m_i^2)$. Clearly, v_0^2 will be

JHEP06(2015)033

modified by this procedure. The validity of the on-shell approximation used in the first step necessitates the effect on v_0^2 to be negligible. This can be translated into the following conditions [22]

$$\frac{v_1^2}{2p_1 \cdot Q_0} \ll \frac{v_0^2}{2p_0 \cdot Q_0} \quad \text{and} \quad \frac{v_2^2}{2p_2 \cdot Q_0} \ll \frac{v_0^2}{2p_0 \cdot Q_0}\,. \tag{2.65}$$

Up to normalization, the terms $\frac{v_l^2}{2p_l \cdot Q_0}$ are equal to Λ_l^2. A similar discussion holds for the initial state shower. We note that one of the consequences of Λ_l^2 ordering is an enlarged phase space for initial state splittings compared to p_T ordering.

2.8 Consequences of backward evolution

Initial state splittings are generated by the backward evolution formalism first introduced by Sjöstrand in refs. [2, 3]. In this approach, the Sudakov form factor contains a ratio of parton distribution functions to guide the evolution of the momentum fraction during splitting. Nevertheless, as long as mass effects are neglected and the splitting functions used in the shower and PDF evolution are the same, one can factor out the non-perturbative part completely. This matches the treatment of final state radiation, where hadronization only happens after showering. Unfortunately, the splitting functions used in the Nagy-Soper parton shower are very different from those of Altarelli-Parisi away from the collinear limit. Thus, non-perturbative information will inevitably affect the evolution.

In the presence of mass effects, however, the non-perturbative input can not be factorized, independently of the approach to the parton shower (traditional or otherwise), unless the evolution of PDFs is modified. We describe the required modification after ref. [23], which has been implemented in Deductor.

In principle we would like to decompose the density matrix as

$$|\rho) = \mathcal{L}(t)|\rho_{\text{pert}})\,, \tag{2.66}$$

where $|\rho_{\text{pert}})$ would contain no non-perturbative information if splittings were restricted to the quasi-collinear limit. Here, the luminosity operator $\mathcal{L}(t)$ is

$$\mathcal{L}(t)|\Phi_m) \equiv \frac{f_{a/A}(\eta_a, \mu_A^2 e^{-t}) f_{b/B}(\eta_b, \mu_B^2 e^{-t})}{4 n_c(a) n_c(b) 4 \eta_a \eta_b p_A \cdot p_B} |\Phi_m)\,, \tag{2.67}$$

where we used a shorthand notation for the statistical states, $\Phi_\lambda = \{p, f, s', c', s, c\}_\lambda$. The scale μ_i^2 is given by $\mu_i^2 = 2p_i \cdot Q_0$, where p_i are the hadron momenta and Q_0 the total final state momentum. Therefore, the PDFs are evaluated at the scale $\mu_i^2 e^{-t} = |(\hat{p}_i - \hat{p}_{m+1})^2 - m_i^2|$ which is the virtuality of the splitting. Let us define a perturbative real splitting operator, $\mathcal{H}_I^{\text{pert}}(t)$, through

$$\mathcal{H}_I(t) = \mathcal{L}(t)\mathcal{H}_I^{\text{pert}}(t)\mathcal{L}^{-1}(t)\,. \tag{2.68}$$

Unfortunately, $\mathcal{V}(t)$ contains a convolution of splitting functions with PDFs, because it is an integral of eq. (2.68). It is thus impossible to trivially factor out the non-perturbative contribution. Nevertheless, we can define a quasi-perturbative virtual splitting operator, $\mathcal{V}^{\text{pert}}(t)$, via the evolution equation. Indeed, substituting eq. (2.66) in eq. (2.22) we obtain

$$\left(\frac{d}{dt}\mathcal{L}(t)\right)|\rho_{\text{pert}}) + \mathcal{L}(t)\left(\frac{d}{dt}|\rho_{\text{pert}})\right) = \left[\mathcal{H}_I(t) - \mathcal{V}(t)\right]\mathcal{L}(t)|\rho_{\text{pert}})\,. \tag{2.69}$$

JHEP06(2015)033

This allows us to write

$$\frac{d}{dt}|\rho_{\rm pert}) = \left[\mathcal{H}_I^{\rm pert}(t) - \mathcal{V}^{\rm pert}(t)\right]|\rho_{\rm pert})\,, \tag{2.70}$$

with

$$\mathcal{V}^{\rm pert}(t) = \mathcal{V}(t) + \mathcal{L}^{-1}(t)\left(\frac{d}{dt}\mathcal{L}(t)\right)\,, \tag{2.71}$$

where we used the fact that $\mathcal{L}(t)$ commutes with $\mathcal{V}(t)$ since it does not change the momenta.

To ensure that $\mathcal{V}^{\rm pert}(t)$ is independent of PDFs in the quasi-collinear limit, the splitting functions obtained by deriving $\mathcal{L}(t)$ must match the quasi-collinear limit of $\mathcal{V}(t)$. The respective functions are given in ref. [23]. As expected, they only differ from the Altarelli-Parisi kernels at non-zero mass. They also imply a modified evolution of the PDFs. The effect is mostly visible on the b-quark PDF. Clearly, only processes predominantly generated from initial state b-quarks will be influenced.

Modifying the evolution of parton distribution functions may be used for other purposes as well. For instance, adding a higher order term $P_{a\hat{a}}^{(2)}$ as follows

$$\begin{aligned}\frac{df_{a/A}(\eta_a,\mu^2)}{d\log(\mu^2)} = &\sum_{\hat{a}}\int\frac{dz}{z}\frac{\alpha_s(\mu^2/z)}{2\pi}P_{a\hat{a}}(z,\mu^2/z)f_{\hat{a}/A}(\eta_a/z,\mu^2)\\ &+\sum_{\hat{a}}\int\frac{dz}{z}\left(\frac{\alpha_s(\mu^2/z)}{2\pi}\right)^2 P_{a\hat{a}}^{(2)}(z,\mu^2/z)f_{\hat{a}/A}(\eta_a/z,\mu^2)\,,\end{aligned} \tag{2.72}$$

with

$$P_{a\hat{a}}^{(2)}(z,\mu^2/z) = -2\pi\beta_0\log(\lambda_R)P_{a\hat{a}}(z,\mu^2/z)\,, \tag{2.73}$$

where $\beta_0 = (33-2n_f)/(12\pi)$ and

$$\lambda_R = \exp\left(-\frac{C_A(67-3\pi^2)-10n_f}{3(33-2n_f)}\right)\,, \tag{2.74}$$

where n_f is the number of light active flavours, allows to incorporate the cusp anomalous dimension at NLL for processes with less then three coloured particles [48].

2.9 A summary of ambiguities

Let us conclude this section with a list of ambiguous components of the Nagy-Soper parton shower:

1. Momentum Mappings
2. Splitting functions
3. Soft partition function
4. Colour treatment
5. Spin treatment
6. Shower time
7. PDF evolution

JHEP06(2015)033

We stress that this shower is a rather recent construction still under development. It is to be expected that there will be changes to any of the particular solutions discussed in the previous subsections.

3 Matching NLO matrix elements to the parton shower

Matching NLO calculations with parton showers is a widely explored subject and there exist several matching schemes, the most popular being POWHEG [28, 29] and MC@NLO [26, 27] (for other proposals see e.g. [13, 49–56]). A general comparison between these two can be found in e.g. [57]. In order to benefit from the recently implemented subtraction scheme based on the Nagy-Soper parton shower splitting kernels [33], we chose the MC@NLO formalism. Notice, that the implementation of MC@NLO in SHERPA [57] also benefits from the consistency between the parton shower (Catani-Seymour) and subtraction terms in the matching. However, once the implementation of the Nagy-Soper parton shower will be made accurate at subleading terms in the colour expansion, our matching procedure will allow for a similar accuracy in the matched sample. This may also be possible in the future within SHERPA, see ref. [11]. Before we discuss the challenges of parton shower matching, we give a brief overview of the general objectives.

Preserving the NLO cross section normalization: when considering an inclusive observable F, the fixed order normalization of the cross section should be preserved. We thus require

$$(F|\mathrm{U}(t_F, t_0)|\rho(t_0)) = \sigma^{\mathrm{NLO}}[F]\,. \tag{3.1}$$

Defining event samples at NLO level: matching to parton shower is the only way to define events at NLO. As we will see, matching *à la* MC@NLO imposes a shower specific subtraction scheme. Without matching, the weights of the real matrix element and the subtraction terms are not coupled kinematically unless in a strict limit, and diverge separately. Due to the matching scheme those weights are combined and one obtains real emission phase space configurations with a finite, but not necessarily positive, weight. The matching renders the virtual corrections finite as well.

Next-to-Leading Logarithmic accuracy for infrared sensitive observables: infrared sensitive observables, which are affected by large logarithms, L, of some kinematic variable at fixed-order, are replaced by resummed predictions. Traditional parton showers only resum the leading logarithms (LL) $\alpha_s^n L^{2n}$, whereas the Nagy-Soper shower also allows to resum the next-to-leading logarithms (NLL) $\alpha_s^n L^{2n-1}$. Therefore, we require differential distributions to be accurate at the NLO+NLL level.

High p_T emissions according to matrix elements: the parton shower is valid in the soft and collinear regimes, the description of high p_T emissions is, therefore, not reliable. On the other hand, NLO calculations are valid in this region. It is desirable to recover the NLO prediction for high p_T emissions despite applying the parton shower.

Connection to low energy physics: the parton evolution down to a low scale allows to include non-perturbative phenomena due to hadronization and multiple interactions.

JHEP06(2015)033

3.1 The quantum density matrix at next-to-leading order

For a generic $2 \to m$ process at NLO, one can write the quantum density matrix in a perturbative expansion in α_s, according to

$$|\rho) = \underbrace{|\rho_m^{(0)})}_{\text{Born, } \mathcal{O}(1)} + \underbrace{|\rho_m^{(1)})}_{\text{Virtual, } \mathcal{O}(\alpha_s)} + \underbrace{|\rho_{m+1}^{(0)})}_{\text{Real, } \mathcal{O}(\alpha_s)} + \mathcal{O}(\alpha_s^2)\,. \tag{3.2}$$

Note that we count the leading order contribution as order 1 in the strong coupling α_s. $|\rho_m^{(0)})$ and $|\rho_{m+1}^{(0)})$ are tree level matrix elements, whereas $|\rho_m^{(1)})$ is the one-loop amplitude. The definitions of these densities are analogous to the definition given in eq. (2.12). So far eq. (3.2) suffers from infrared divergences, however, the expansion of $|\rho)$ in α_s is defined within dimensional regularization. Based on this quantum density matrix, the expectation value of the observable F including shower effects reads

$$\sigma[F]^{\text{PS}} = (F|\mathrm{U}(t_F, t_0)|\rho) = \sum_{\lambda=m}^{\infty} \frac{1}{\lambda!} \int [d\Phi_\lambda](F|\Phi_\lambda)(\Phi_\lambda|\mathrm{U}(t_F, t_0)|\rho)\,, \tag{3.3}$$

where $\Phi_\lambda = \{p, f, s', c', s, c\}_\lambda$. The quantum density $|\rho)$ accounts for the hard matrix elements for $\lambda = m$ and $\lambda = m+1$. This naive description of the cross section suffers from double counting, as we will show using the iterative solution to the evolution equation expanded to $\mathcal{O}(\alpha_s)$. Indeed, there is

$$|\rho(t_F)) = \mathrm{U}(t_F, t_0)|\rho) \approx |\rho) + \int_{t_0}^{t_F} d\tau \left[\mathcal{H}_I(\tau) - \mathcal{V}(\tau)\right] |\rho_m^{(0)}) + \mathcal{O}(\alpha_s^2)\,. \tag{3.4}$$

As we can see from the unitarity condition $(1|\left[\mathcal{H}_I(\tau) - \mathcal{V}(\tau)\right] = 0$, the total cross section $(1|\rho(t_F))$ is conserved. On the other hand, one does not recover the NLO prediction for inclusive observables F because in general $(F|\left[\mathcal{H}_I(\tau) - \mathcal{V}(\tau)\right] \neq 0$. Even without this requirement the result is not correct, since it contains the first emission contributions twice, once from the real emission quantum density $|\rho_{m+1}^{(0)})$, and once from the parton shower approximation $\mathcal{H}_I(\tau)|\rho_m^{(0)})$. We will now show how to overcome this problem.

3.2 Matching fully inclusive processes to parton shower

Let us begin with a class of processes, which have a well defined total cross section at leading order, e.g. $pp \to t\bar{t}$ or $pp \to W^+W^-$. Working along the line of the MC@NLO scheme, we notice that the additional parton shower contribution in eq. (3.4) can be cancelled by including appropriate counterterms. Let us, therefore, introduce the following modified quantum density matrix

$$|\bar{\rho}) \equiv |\rho) - \int_{t_0}^{t_F} d\tau \left[\mathcal{H}_I(\tau) - \mathcal{V}(\tau)\right] |\rho_m^{(0)}) + \mathcal{O}(\alpha_s^2)\,. \tag{3.5}$$

The total cross section $(1|\bar{\rho}) = (1|\rho) = \sigma^{\text{NLO}}$ is unchanged, due to the unitarity condition. On the other hand, considering $\mathrm{U}(t_F, t_0)|\bar{\rho})$ and expanding the evolution equation shows that the undesired parton shower contributions are cancelled up to $\mathcal{O}(\alpha_s)$. This cancellation

JHEP06(2015)033

is non-trivial, because the modified quantum density matrix $|\bar{\rho})$, now depends explicitly on the parton shower splitting kernels, the momentum mappings, the ordering of the emissions and the choice of the starting shower time t_0.

For an infrared safe observable F, we have

$$\begin{aligned}\bar{\sigma}[F] = \frac{1}{m!}\int [d\Phi_m](F|\mathrm{U}(t_F,t_0)|\Phi_m)\left[(\Phi_m|\rho_m^{(0)})+(\Phi_m|\rho_m^{(1)})+\int_{t_0}^{t_F} d\tau(\Phi_m|\mathcal{V}(\tau)|\rho_m^{(0)})\right] \\ +\frac{1}{(m+1)!}\int [d\Phi_{m+1}](F|\mathrm{U}(t_F,t_0)|\Phi_{m+1})\left[(\Phi_{m+1}|\rho_{m+1}^{(0)})-\int_{t_0}^{t_F} d\tau(\Phi_{m+1}|\mathcal{H}_I(\tau)|\rho_m^{(0)})\right].\end{aligned} \tag{3.6}$$

In the MC@NLO approach, the parton shower splitting kernels are used to provide subtraction terms for the infrared divergences in $|\rho_m^{(1)})$ and $|\rho_{m+1}^{(0)})$. Thus, the infrared cutoff t_F may be removed by taking the limit $t_F \to \infty$. Even though this is a source of a mismatch between the fixed order and the shower calculation, it is numerically small due to the exponential damping by the Sudakov form factor as discussed in ref. [2]. In the real subtracted cross section, described in the second line of eq. (3.6), we use the definition of the real splitting operator from eq. (2.36) and write

$$\int_{t_0}^{\infty} d\tau\ \mathcal{H}_I(\tau) = \sum_l \mathbf{S}_l \int_0^{\infty} d\tau\ \delta(\tau - t_l)\Theta(\tau - t_0) = \sum_l \mathbf{S}_l \Theta(t_l - t_0)\,. \tag{3.7}$$

Here the sum runs over all external legs and $\mathbf{S}_l$ is the total splitting kernel for a given external leg l. We want to emphasize that $\mathbf{S}_l$ also contains non-singular contributions like the massive $g \to Q\bar{Q}$ splitting. Therefore, the operator $\mathcal{H}_I(t)$ contains more than is needed for a subtraction scheme. The parameter t_l is the shower time defined in section 2.7. Hence, $\Theta(t_l - t_0)$ represents the ordering of the emissions and the t_0 dependence introduces a dynamical restriction of the subtraction phase space. The choice of t_0 will be discussed at the end of this chapter, because it has non-trivial consequences. The real subtracted cross section is finite in $d = 4$ dimensions, as t_l is allowed to approach infinity.

Integrating the virtual operator $\mathcal{V}(\tau)$ without an infrared cutoff is more complex, considering that there is an explicit integration over the splitting variables. Hence, we have to integrate this part in $d = 4 - 2\epsilon$ dimensions analytically to extract the $1/\epsilon^2$ and $1/\epsilon$ poles. The integrated virtual operator takes the form

$$\int_{t_0}^{\infty} d\tau\ \mathcal{V}(\tau) = \sum_l \int d\Gamma_l\ \mathbf{S}_l \Theta(t_l - t_0) \equiv \mathbf{I}(t_0) + \mathbf{K}(t_0)\,, \tag{3.8}$$

where $d\Gamma_l$ is the phase space integration of the additional parton. The decomposition of the integrated $\mathcal{V}(\tau)$ into two operators $\mathbf{I}(t_0)$ and $\mathbf{K}(t_0)$ is arbitrary. However, we choose $\mathbf{I}(t_0)$ to match the divergencies of the virtual amplitude, as it is customary. We emphasize this structure to illustrate that the parton shower naturally incorporates a subtraction scheme similar to the Catani-Seymour framework [14, 15]. In the case of initial state partons it is necessary to include additional collinear counterterms, denoted by $\mathbf{P}$, needed for the

JHEP06(2015)033

renormalization of the parton distribution functions. Thus, the matched cross section reads

$$\bar{\sigma}[F] = \int \frac{[d\Phi_m]}{m!}(F|\mathrm{U}(t_F,t_0)|\Phi_m)\left[(\Phi_m|\rho_m^{(0)}) + (\Phi_m|\rho_m^{(1)}) + (\Phi_m|[\mathbf{I}(t_0)+\mathbf{K}(t_0)+\mathbf{P}]|\rho_m^{(0)})\right] + \int \frac{[d\Phi_{m+1}]}{(m+1)!}(F|\mathrm{U}(t_F,t_0)|\Phi_{m+1})\left[(\Phi_{m+1}|\rho_{m+1}^{(0)}) - \sum_l (\Phi_{m+1}|\mathbf{S}_l|\rho_m^{(0)})\Theta(t_l-t_0)\right]. \quad (3.9)$$

For future reference, let us define the shorthands, as in ref. [26]:

$$(\Phi_m|S) \equiv (\Phi_m|\rho_m^{(0)}) + (\Phi_m|\rho_m^{(1)}) + (\Phi_m|[\mathbf{I}(t_0)+\mathbf{K}(t_0)+\mathbf{P}]|\rho_m^{(0)})\,, \quad (3.10)$$

$$(\Phi_{m+1}|H) \equiv (\Phi_{m+1}|\rho_{m+1}^{(0)}) - \sum_l (\Phi_{m+1}|\mathbf{S}_l|\rho_m^{(0)})\Theta(t_l-t_0)\,. \quad (3.11)$$

The total cross section is then given by

$$\bar{\sigma}^{\mathrm{NLO}}[1] = \frac{1}{m!}\int [d\Phi_m](1|\Phi_m)(\Phi_m|S) + \frac{1}{(m+1)!}\int [d\Phi_{m+1}](1|\Phi_{m+1})(\Phi_{m+1}|H)\,, \quad (3.12)$$

whereas including parton shower evolution amounts to the integrals

$$\bar{\sigma}[F]^{\mathrm{PS}} = \frac{1}{m!}\int [d\Phi_m](F|\mathrm{U}(t_F,t_0)|\Phi_m)(\Phi_m|S) + \frac{1}{(m+1)!}\int [d\Phi_{m+1}](F|\mathrm{U}(t_F,t_0)|\Phi_{m+1})(\Phi_{m+1}|H)\,. \quad (3.13)$$

Matching is a two step procedure, which consists of first generating the samples according to eq. (3.10) and (3.11), followed by the application of $\mathrm{U}(t_F,t_0)$.

3.3 Matching in the presence of singularities in the born approximation

For processes with massless partons at leading order, the matching prescription as described in eq. (3.9) must be slightly modified by the inclusion of generation cuts, as discussed for example in refs. [58, 59]. A naive modification to the matching prescription would be to make the following replacements

$$(\Phi_m|S) \to (\Phi_m|S)F_I(\{\hat{p},\hat{f}\}_m)\,, \quad (3.14)$$

$$(\Phi_{m+1}|H) \to (\Phi_{m+1}|H)F_I(\{p,f\}_{m+1})\,, \quad (3.15)$$

where $F_I(\{p,f\}_\lambda)$ is a jet function applied during the generation of events, on the momenta and flavours of Φ_λ. Applying the parton shower to these ensembles shows that double counting is not removed. Indeed, substituting eq. (3.14) and eq. (3.15) in eq. (3.13) we obtain

$$\bar{\sigma}[F]^{\mathrm{PS}} = \frac{1}{m!}\int [d\Phi_m](F|\mathrm{U}(t_F,t_0)|\Phi_m)(\Phi_m|S)F_I(\{\hat{p},\hat{f}\}_m) + \frac{1}{(m+1)!}\int [d\Phi_{m+1}](F|\mathrm{U}(t_F,t_0)|\Phi_{m+1})(\Phi_{m+1}|H)F_I(\{p,f\}_{m+1})\,. \quad (3.16)$$

JHEP06(2015)033

Expanding the evolution operator, as given by eq. (3.4), yields

$$\begin{aligned}\bar{\sigma}[F]^{\mathrm{PS}} \approx & \frac{1}{m!}\int [d\Phi_m](F|\Phi_m)(\Phi_m|\left[|\rho_m^{(0)}) + |\rho_m^{(1)}) + \mathbf{P}|\rho_m^{(0)})\right] F_I(\{\hat{p},\hat{f}\}_m) \\ & + \frac{1}{(m+1)!}\int [d\Phi_{m+1}](F|\Phi_{m+1})(\Phi_{m+1}|\rho_{m+1}^{(0)})F_I(\{p,f\}_{m+1}) \\ & + \int \frac{[d\Phi_m]}{m!}\frac{[d\Phi_{m+1}]}{(m+1)!}\int_{t_0}^{t_F} d\tau\ (F|\Phi_{m+1})(\Phi_{m+1}|\mathcal{H}_I(\tau)|\Phi_m) \\ & \times (\Phi_m|\rho_m^{(0)})\Big[F_I(\{\hat{p},\hat{f}\}_m) - F_I(\{p,f\}_{m+1})\Big] + \mathcal{O}(\alpha_s^2)\,,\end{aligned} \tag{3.17}$$

where the $\mathbf{I}(t_0) + \mathbf{K}(t_0)$ contribution of $(\Phi_m|S)$ has been cancelled by the linear expansion of the Sudakov form factor. The offending term is present in the 3rd and 4th lines of eq. (3.17). It does not vanish because $F_I(\{\hat{p},\hat{f}\}_m)$ is not equal to $F_I(\{p,f\}_{m+1})$ for non-singular configurations, despite the fact that their momenta and flavours are related according to $\{p,f\}_{m+1} = R_l(\{\hat{p},\hat{f}\}_m, \Gamma_l, \chi_l)$. The mismatch can be cured by enforcing the subtraction terms to fulfill $F_I(\{\hat{p},\hat{f}\}_m)$, i.e. by modifying the real subtracted cross section according to

$$\begin{aligned}&(\Phi_{m+1}|H) \longrightarrow \\ &(\Phi_{m+1}|\tilde{H}) \equiv \big(\Phi_{m+1}|\rho_{m+1}^{(0)}\big) - \sum_l (\Phi_{m+1}|\mathbf{S}_l|\rho_m^{(0)})\Theta(t_l - t_0)F_I(Q_l(\{p,f\}_{m+1}))\,,\end{aligned} \tag{3.18}$$

where we make use of the inverse momentum mapping Q_l, as defined in eq. (2.30). Thus,

$$F_I(Q_l(\{p,f\}_{m+1})) = F_I(\{\hat{p},\hat{f}\}_m)\,. \tag{3.19}$$

This modification allows us to compute cross sections with massless partons, at the same time introducing restrictions on the functional form of F_I. Using eq. (3.18) in addition to eq. (3.15) in the definition of the cross section in eq. (3.13) and expanding the shower evolution yields

$$\begin{aligned}\bar{\sigma}[F]^{\mathrm{PS}} \approx & \frac{1}{m!}\int [d\Phi_m](F|\Phi_m)(\Phi_m|\left[|\rho_m^{(0)}) + |\rho_m^{(1)}) + \mathbf{P}|\rho_m^{(0)})\right] F_I(\{\hat{p},\hat{f}\}_m) \\ & + \frac{1}{(m+1)!}\int [d\Phi_{m+1}](F|\Phi_{m+1})(\Phi_{m+1}|\rho_{m+1}^{(0)})F_I(\{p,f\}_{m+1}) \\ & + \int \frac{[d\Phi_m]}{m!}\frac{[d\Phi_{m+1}]}{(m+1)!}\int_{t_0}^{t_F} d\tau\ (F|\Phi_{m+1})(\Phi_{m+1}|\mathcal{H}_I(\tau)|\Phi_m) \\ & \times (\Phi_m|\rho_m^{(0)})\Big[1 - F_I(\{p,f\}_{m+1})\Big]F_I(\{\hat{p},\hat{f}\}_m) + \mathcal{O}(\alpha_s^2)\,.\end{aligned} \tag{3.20}$$

The double counting is removed from eq. (3.20), if the following condition is satisfied

$$\Big[1 - F_I(\{p,f\}_{m+1})\Big]F(\{p,f\}_{m+1}) = 0\,, \tag{3.21}$$

where we have used the fact that $(F|\Phi_{m+1}) \sim F(\{p,f\}_{m+1})$. This is achieved if

$$F_I(\{p,f\}_{m+1}) = 1\,,\ \text{for}\ F(\{p,f\}_{m+1}) \neq 0\,, \tag{3.22}$$

JHEP06(2015)033

and can be understood as the generation cuts $F_I(\{p,f\}_{m+1})$ being more inclusive than cuts that are applied on the final observable $F(\{p,f\}_{m+1})$.

Our previous discussion of double counting relied on the fact that the splitting functions were the same in the NLO subtraction scheme and in the parton shower. However, in the case of initial state splittings, this is not the case due to mass effects and the presence of different PDFs. The parton shower PDFs are evolved as explained in section 2.8 using modified leading order splitting kernels. On the other hand, the fixed order calculation employs NLO PDFs. We point out that the implied mismatch is of order $\mathcal{O}(\alpha_s^2)$ as long as both PDF sets are equal at some scale. This means that we use an NLO PDF parameterization as an input for the parton shower PDF evolution. A second source of mismatch is the treatment of mass effects in the initial state. In the case of the parton shower, the splitting kernels are modified as explained in section 2.8, whereas the specifics of the treatment of mass thresholds depends on the PDF collaboration [60].

Finally, let us note that a last source of mismatch is due to scales in the strong coupling constant in the subtraction terms and in the shower. However, just like in the case of PDF evolution, it is of higher order.

3.4 On-shell projection

As mentioned before, the Nagy-Soper parton shower allows for massive initial state partons and treats the charm and bottom quarks as massive. In an NLO calculation the charm quark is usually assumed massless, whereas the bottom quark is only present in the initial state if it is massless as well, which corresponds to the 5-flavour scheme. The practical application of the matching procedure requires, therefore, an on-shell projection for charm and bottom quarks. We use different procedures in the initial and final state cases.

Initial state quarks. We proceed iteratively by making one quark massive at a time. For definiteness, we will modify p_a which is assumed to have $p_a^2 = 0$, whereas the mass, m_b, of p_b is arbitrary. The total momentum is given by

$$Q = p_a + p_b \,, \tag{3.23}$$

where

$$p_a = \eta_a p_A \,, \qquad p_b = \eta_b p_B + \frac{m_b^2}{\eta_b s} p_A \,, \tag{3.24}$$

with η_a and η_b the momentum fractions, $p_{A/B}$ the hadron momenta and $s = 2(p_A \cdot p_B)$ the hadronic center of mass energy squared. This can be written as

$$Q = \left(\eta_a + \frac{m_b^2}{\eta_b s}\right) p_A + \eta_b p_B \,, \qquad Q^2 = s\eta_a\eta_b + m_b^2 \,. \tag{3.25}$$

We shall determine $\hat{\eta}_a$, such that

$$\hat{p}_a = \hat{\eta}_a p_A + \frac{m_a^2}{\hat{\eta}_a s} p_B \,, \quad \hat{p}_a^2 = m_a^2 \neq 0 \,. \tag{3.26}$$

The new total momentum $\hat{Q} = \hat{p}_a + p_b$ and its invariant mass then read

$$\begin{aligned} \hat{Q} &= \left(\hat{\eta}_a + \frac{m_b^2}{\eta_b s}\right) p_A + \left(\eta_b + \frac{m_a^2}{\hat{\eta}_a s}\right) p_B \,, \\ \hat{Q}^2 &= s\eta_b\hat{\eta}_a + \frac{m_b^2 m_a^2}{s\eta_b\hat{\eta}_a} + m_b^2 + m_a^2 \,. \end{aligned} \tag{3.27}$$

The requirement, $\hat{Q}^2 = Q^2$, yields

$$\hat{\eta}_a = \eta_a \left(\frac{1}{2} - \frac{m_a^2}{2Q^2} + \frac{\sqrt{(m_a^2 - Q^2)^2 - 4m_a^2 m_b^2}}{2Q^2} \right) . \tag{3.28}$$

To ensure total momentum conservation, the complete final state has to be boosted in the z-direction. The rapidity of the boost, ω, is

$$e^\omega = \frac{Q^2 + m_b^2 - m_a^2}{2m_b^2} - \frac{\sqrt{\left(Q^2 + m_b^2 - m_a^2\right)^2 - 4Q^2 m_b^2}}{2m_b^2} \,, \tag{3.29}$$

which for $m_b = 0$ reduces to

$$e^\omega = \frac{Q^2}{Q^2 - m_a^2} \,. \tag{3.30}$$

Final state quarks. In the case of a final state massless quark with momentum p_l, we exploit the momentum mapping procedure of the Nagy-Soper parton shower to generate a non-zero mass m_l. The new momentum is given by

$$\hat{p}_l = \lambda p_l + \frac{1 - \lambda + y}{2a_l} Q \,, \qquad \hat{p}_l^2 = m_l^2 \,, \tag{3.31}$$

where Q is the total final state momentum and

$$a_l = \frac{Q^2}{2p_l \cdot Q} \,, \qquad b_l = \frac{m_l^2}{2p_l \cdot Q} \,. \tag{3.32}$$

The parameter y is determined by requiring that the invariant mass of the total recoiling momentum, $K = Q - p_l$, be preserved, i.e. $K^2 = \hat{K}^2$, with $\hat{K} = Q - \hat{p}_l$. The result is

$$y = b_l \,. \tag{3.33}$$

As a consequence, K and $\hat{K}$ are connected by a boost [16] given by

$$\mathcal{B}^{\mu\nu} = g^{\mu\nu} - 2\frac{(K + \hat{K})^\mu (K + \hat{K})^\nu}{(K + \hat{K})^2} + 2\frac{\hat{K}^\mu K^\nu}{K^2} \,. \tag{3.34}$$

The parameter λ is determined by the on-shell condition $\hat{p}_l^2 = m_l^2$, which yields

$$\lambda = \sqrt{(1 + y)^2 - 4a_l b_l} \,, \tag{3.35}$$

which is well-defined if

$$p_l \cdot Q > m_l \left(\sqrt{Q^2} - \frac{m_l}{2} \right) . \tag{3.36}$$

JHEP06(2015)033

In the center-of-mass frame of Q, this becomes

$$E_l > m_l\left(1 - \frac{m_l}{2\sqrt{Q^2}}\right). \tag{3.37}$$

Clearly, arbitrarily soft quarks cannot be projected on the mass-shell.

In case of $2 \to 2$ processes, $a_l = 1$ and the boost in eq. (3.34) is singular. In that case one can use an alternative boost [16]

$$\mathcal{B}^{\mu\nu} = g^{\mu\nu} + \left(\frac{K\cdot n}{\hat{K}\cdot n} - 1\right) n^\mu \bar{n}^\nu + \left(\frac{\hat{K}\cdot n}{K\cdot n} - 1\right) \bar{n}^\mu n^\nu\,, \tag{3.38}$$

with

$$n = \sqrt{\frac{2}{Q^2}}\, p_l\,, \qquad \bar{n} = \sqrt{\frac{2}{Q^2}}\, (Q - p_l)\,. \tag{3.39}$$

3.5 Initial conditions for the parton shower

As described in section 2.7, the shower evolution emissions are strongly ordered in the parameter Λ_l^2, which is related to the shower time t as follows,

$$e^{-t} = \frac{\Lambda_l^2}{Q_0^2}\,, \qquad \Lambda_l^2 = \frac{|(\hat{p}_l \pm \hat{p}_{m+1})^2 - m_l^2|}{2p_l\cdot Q_0} Q_0^2\,, \tag{3.40}$$

where p_l is the emitter momentum and Q_0 is the total final state momentum before emission. The emitter momentum after emission is $\hat{p}_l$, while $\hat{p}_{m+1}$ is the momentum of the emitted particle. The parton shower evolution starts at an initial time t_0, which has to be determined by the user. Since the choice of t_0 has a noticable influence on the differential distributions, it is necessary to provide a sensible prescription, which is the purpose of this section.

Consider first a process at leading order, e.g. $pp \to t\bar{t}$. The parton shower will generate additional radiation. However, the resulting hard jets are described very poorly, because the parton shower description is only valid close to infrared limits. As a consequence, the p_T distribution of the top quark pair is not reliably reproduced for large values of the transverse momentum. Since the initial time t_0 restricts the available phase space for parton emissions, it will have a strong influence on the distribution, as reported, for example, in ref. [61]. Notice that the situation may be improved with merging of different multiplicity samples, see ref. [62].

Matching at NLO has the advantage of providing one hard emission exactly through the matrix element. According to our modified quantum density matrix, we removed all parton shower contributions to the first emission. Therefore, corrections to the p_T distribution are formally of higher order, even though they can be a priori large [57, 63]. The ultimate goal is to choose t_0 such that the description of the high p_T regime is close to that of the NLO fixed order approximation. This can be achieved by restricting the parton shower phase space to allow only splittings with virtualities lower than the splittings already present in the hard matrix element.

JHEP06(2015)033

We choose t_0 to approximate the virtuality of the hard process on an event-by-event basis. Inspired by refs. [27, 64], we define

$$e^{-t_0} = \min_{i \neq j} \left\{ \frac{2p_i \cdot p_j}{Q_0^2} \right\} , \tag{3.41}$$

where p_i and p_j are pairwise different external momenta of the process considered.

For the real radiation contribution, we use the subtraction terms eq. (3.18) to determine t_0 as follows

1. For each subtraction term

$$(\Phi_{m+1}|\mathbf{S}_l|\rho_m^{(0)})\Theta(t_l - t_0)F_I(Q_l(\{p,f\}_{m+1})) , \tag{3.42}$$

   determine its individual t_0 according to eq. (3.41) while t_l according to eq. (3.40). Retain t_l if $t_l > t_0$.

2. If there is at least one t_l, then evaluate t_0 according to

$$e^{-t_0} = \min_l \left(e^{-t_l}\right) , \tag{3.43}$$

   where the minimum runs over all t_l found in the previous step.

3. Otherwise, apply eq. (3.41) to the $(m+1)$-particle kinematics.

Let us note that the separate determination of t_0 in step 1 for each subtraction term, is necessary to avoid double counting.

3.6 A summary of ambiguities

In this section, we recapitulate by listing the intrinsic uncertainties introduced by the MC@NLO matching formalism in combination with the Nagy-Soper parton shower.

Parton distribution functions: parton distribution functions are evolved differently in the NLO calculation and in the parton shower. Nevertheless, we pointed out in section 3.3, that the evolution itself is of higher order. Thus, the NLO accuracy is obtained as long as the evolutions share a common point, e.g. at the low scale.

Parton masses: a generic feature of the Nagy-Soper parton shower is that it requires massive bottom and charm quarks in the initial state. However, the fixed order calculation involves massless charm quarks at least. Although the implied mismatch is power suppressed, it is necessary to introduce masses for the relevant quarks in the fixed order sample used as input for the shower. In section 3.4, we have provided a possible algorithm. Nonetheless, other choices might influence the final result.

Initial state shower time: the choice of t_0 in the parton evolution is, to a large extent, arbitrary. The only requirement is that the NLO prediction be recovered for hard emissions. This can be achieved by several different choices of t_0, with either fixed or configuration dependent values. In section 3.5, we have presented our choice, but others are possible. Nevertheless, it is recommended to vary t_0 by rescaling it by a common value within some reasonable range, see section 5.1.

JHEP06(2015)033

4 Implementation

In this section, we present a realization of the matching scheme within the HELAC-NLO framework [65]. Due to the restricted functionality of the Nagy-Soper parton shower present in DEDUCTOR version 1.0.0 [24], which we used as basis for practical studies, our implementation is simplified as far as spin and colour treatments are concerned. Since DEDUCTOR uses spin averaged splitting functions, we only provide unpolarized event samples for showering. On the other hand, we supply only leading colour events even though DEDUCTOR works with the LC+ approximation and may shower non-diagonal colour configurations. While proper colour matching does not present conceptual challenges, it requires some additional programming effort. The latter will be necessary once DEDUCTOR has full colour functionality. We believe that, for a first study, our simplification is justified. More details on our approach can be found in appendix A. Finally, we note that, at present, DEDUCTOR lacks unstable particle decays and a hadronization model.

4.1 Modifications in HELAC-DIPOLES

The implementation of the matching scheme in the HELAC-NLO multi-purpose event generator only concerns HELAC-DIPOLES [33, 35]. We base our work on the previous implementation [33], where the majority of the parton shower operators $\mathcal{H}_I$ and $\mathcal{V}$ have already been included.

Momentum mapping for initial state splitting. The momentum mapping implemented in HELAC-DIPOLES is based on ref. [16]. For reasons, which we shortly discussed in section 2.4, the mapping implemented in DEDUCTOR is slightly different [19]. Here, we reproduce the necessary formulae used in the new version of HELAC-DIPOLES.

We start from a set of momenta $\{\tilde{p}\}_m$ and consider the splitting $\tilde{p}_a \to p_a + p_{m+1}$. The incoming momenta are given by

$$\tilde{p}_a = \tilde{\eta}_a P_A \,, \qquad \tilde{p}_b = \tilde{\eta}_b P_B \,, \tag{4.1}$$

where P_A and P_B are the hadron momenta. After the splitting, there is

$$p_a = \frac{1}{z}\tilde{p}_a \,, \quad p_b = \tilde{p}_b \,, \tag{4.2}$$

and the momentum p_{m+1} of the emitted particle is parametrized by

$$p_{m+1} = x_a \tilde{p}_a + x_b \tilde{p}_b + k_\perp \,, \tag{4.3}$$

where

$$|k_\perp|^2 = 2 x_a x_b (\tilde{p}_a \cdot \tilde{p}_b) \,, \quad x_a = \frac{1}{z} - 1 - y \,, \quad x_b = zy \,. \tag{4.4}$$

The phase space variables y, z and ϕ are defined as

$$\begin{aligned} z &= \frac{\tilde{\eta}_a}{\eta_a} = \frac{s\tilde{\eta}_a\tilde{\eta}_b}{s\eta_a\eta_b} = \frac{\tilde{Q}^2}{(p_a + p_b)^2} \,, \\ y &= -\frac{(p_a - p_{m+1})^2}{2(\tilde{p}_a \cdot \tilde{p}_b)} = \frac{2p_a \cdot p_{m+1}}{\tilde{Q}^2} \,, \\ \phi &\in [0, 2\pi] \,, \end{aligned} \tag{4.5}$$

where $\tilde{Q} = p_a + p_b - p_{m+1} = \tilde{p}_a + \tilde{p}_b$. To ensure momentum conservation the remaining final state particles have to be boosted, $p_i = \mathcal{B}\tilde{p}_i$, with the Lorentz transformation [22]

$$\begin{aligned}\mathcal{B}^{\mu\nu}(\omega, v_\perp) = g_\perp^{\mu\nu} &+ \frac{e^{\omega}\tilde{p}_a^\mu\tilde{p}_b^\nu + e^{-\omega}\tilde{p}_b^\mu\tilde{p}_a^\nu}{\tilde{p}_a\cdot\tilde{p}_b} \\ &+ \sqrt{\frac{2}{\tilde{p}_a\cdot\tilde{p}_b}}\left[e^{\omega}v_\perp^\mu\tilde{p}_b^\nu - \tilde{p}_b^\mu v_\perp^\nu\right] - e^{\omega}v_\perp^2\frac{\tilde{p}_b^\mu\tilde{p}_b^\nu}{\tilde{p}_a\cdot\tilde{p}_b}\,,\end{aligned} \tag{4.6}$$

where

$$\begin{aligned} g_\perp^{\mu\nu} &= g^{\mu\nu} - \frac{\tilde{p}_a^\mu\tilde{p}_b^\nu + \tilde{p}_b^\mu\tilde{p}_a^\nu}{\tilde{p}_a\cdot\tilde{p}_b}\,, \\ e^{\omega} &= \frac{1}{z} - x_a = 1 + y\,, \\ v_\perp &= -\frac{e^{-\omega}}{\sqrt{2\tilde{p}_a\cdot\tilde{p}_b}}k_\perp\,. \end{aligned} \tag{4.7}$$

In the case, where $\tilde{p}_b$ is the emitter one simply exchanges $\tilde{p}_a$ and $\tilde{p}_b$ in the equations above. This momentum mapping is implemented in the **I** and **KP** operators of the HELAC-DIPOLES package, while the modification only concerns initial-final state interference contributions. For the real subtracted cross section, the inverse transformation has to be applied

$$\begin{aligned} &\tilde{p}_a = z p_a\,, \qquad \tilde{p}_b = p_b\,, \\ &\tilde{p}_i = \mathcal{B}^{-1}p_i \qquad (i = 1, \dots m)\,, \end{aligned} \tag{4.8}$$

with

$$\begin{aligned}\left(\mathcal{B}^{-1}\right)^{\mu\nu}(\omega, v_\perp) = g_\perp^{\mu\nu} &+ \frac{e^{-\omega}\tilde{p}_a^\mu\tilde{p}_b^\nu + e^{\omega}\tilde{p}_b^\mu\tilde{p}_a^\nu}{\tilde{p}_a\cdot\tilde{p}_b} \\ &+ \sqrt{\frac{2}{\tilde{p}_a\cdot\tilde{p}_b}}\left[e^{\omega}\tilde{p}_b^\mu v_\perp^\nu - v_\perp^\mu\tilde{p}_b^\nu\right] - e^{\omega}v_\perp^2\frac{\tilde{p}_b^\mu\tilde{p}_b^\nu}{\tilde{p}_a\cdot\tilde{p}_b}\,.\end{aligned} \tag{4.9}$$

Dynamical phase space restriction. A second modification to the existing subtraction scheme is the implementation of a dynamical cutoff $\Theta(t_l - t_0)$ on the available dipole phase space, which represents the ordering of the emissions in the parton shower evolution. The new subtraction terms read (see section 3.2)

$$\int_{t_0}^{\infty} d\tau\ \mathcal{H}_I(\tau) = \sum_l \mathbf{S}_l\Theta(t_l - t_0)\,, \tag{4.10}$$

where the splitting operator $\mathbf{S}_l$ is already available in HELAC-DIPOLES. The shower time t_l is given by (see section 3.5)

$$e^{-t_l} = \frac{|(\hat{p}_l \pm \hat{p}_{m+1})^2 - m_l^2|}{2p_l\cdot Q_0}\,, \tag{4.11}$$

and can be reconstructed from the $\{\hat{p}, \hat{f}\}_{m+1}$ kinematics. The numerator is given by real radiation momenta, whereas the denominator $2p_l\cdot Q_0$ is given by the momenta before the

JHEP06(2015)033

splitting. However, the denominator can also be reconstructed by making explicit use of the momentum mappings.

This phase space restriction is also implemented in the integrated dipoles. In order to use as much existing code as possible, we implement it in the form of

$$\int_{t_0}^{\infty} d\tau\ V(\tau) = \sum_l \int d\Gamma_l\ \mathbf{S}_l \Theta(t_l - t_0) = \sum_l \int d\Gamma_l\ \mathbf{S}_l \left[1 - \Theta(t_0 - t_l)\right] . \tag{4.12}$$

Therefore, we can calculate the finite remainder in $d = 4$ dimensions and subtract it from the complete expression. We follow closely the outlined semi-numerical strategy presented in [33].

We note that, even though the restriction is necessary for matching, it can be also used in fixed order NLO calculation as an effective cutoff on the subtraction phase space similar to $\alpha_{\max}$ in the Catani-Seymour subtraction scheme [66–68].

4.2 Monte Carlo techniques

With the modifications described above, it is possible to use HELAC-NLO to generate an event sample ready for showering with DEDUCTOR. We produce events subprocess by subprocess. First, we use HELAC-1LOOP [69] to obtain a set of unweighted leading order events with the virtual contributions

$$\omega_i(\{p,f\}_m) = 1 + \frac{(\{p,f\}_m|\rho_m^{(1)})}{(\{p,f\}_m|\rho_m^{(0)})} , \tag{4.13}$$

where only the finite part of $|\rho_m^{(1)})$ is included. At this point

$$\sigma[\mathrm{LO+V}] = \frac{\sigma[\mathrm{LO}]}{N} \sum_{i=1}^{N} w_i . \tag{4.14}$$

This set of weighted events is subsequently reweighted using HELAC-DIPOLES in order to include the parton shower virtual operator. This corresponds to taking into account the integrated subtraction terms. The weights become

$$\omega_i(\{p,f\}_m) = 1 + \frac{(\{p,f\}_m|\rho_m^{(1)})}{(\{p,f\}_m|\rho_m^{(0)})} + \frac{(\{p,f\}_m|\mathbf{I}(t_0) + \mathbf{K}(t_0) + \mathbf{P}|\rho_m^{(0)})}{(\{p,f\}_m|\rho_m^{(0)})} , \tag{4.15}$$

yielding

$$\sigma[\mathrm{LO+V+I+KP}] = \frac{\sigma[\mathrm{LO}]}{N} \sum_{i=1}^{N} w_i . \tag{4.16}$$

Notice that the integrated subtraction terms are Monte Carlo integrals on the phase space $d\Gamma_l$ of the additional unresolved parton. In order to obtain a good approximate of this integral, we sample several points for a fixed born phase space point $\{p,f\}_m$. This proved to be advantageous in case of large cancellations in $\mathcal{V}(\tau)$.

The real radiation events are generated separately with HELAC-DIPOLES, which was extended to provide unweighted events with positive and negative weights, ± 1 [70]. Notice

JHEP06(2015)033

that unweighting is possible, because both the real radiation and the respective subtraction weights correspond to the same phase space point as described in section 3.2. For each accepted event, we choose the most probable diagonal colour flow with the colour weight

$$C_w(\{p,f,c\}_{m+1}) = \frac{\left(\{p,f,c\}_{m+1}|\rho^{(0)}_{m+1}\right)}{\sum_{\{c'\}_{m+1}}\left(\{p,f,c'\}_{m+1}|\rho^{(0)}_{m+1}\right)}\,. \tag{4.17}$$

The generated events are stored in a Les Houches file [71], with the initial parton shower time t_0 assigned to the variable `SCALEUP`.

4.3 Interface to Deductor

Events generated by Helac-Nlo are transferred to Deductor. This requires an on-shell projection for charm and bottom quarks (see section 3.4) and the determination of a starting colour configuration for each event.

On-shell projection. The on-shell projection of section 3.4 is applied iteratively to each charm and bottom quark. In the case of an initial state transformation for two massless quarks bound to become massive, the order of longitudinal boost is relevant. Indeed, the first boost has a lower rapidity than the second as can be proven by inspection of eqs. (3.29) and (3.30). We choose the order at random in order to reduce the systematics. In case the projection fails, which is only possible for soft bottom and charm quarks in the real radiation contribution, the event is rejected. Vetoing such emissions may only induce a negligible modification of the cross section. Otherwise, effects, which are not under control, would be substantial. This problem has to be studied case-by-case.

Colour configurations. A colour flow generated as described before in the Les Houches [71] format must be translated to the internal representation of Deductor in terms of colour strings, see section 2.1. Notice that only one colour flow is needed in the leading colour approximation per event. A colour flow is given by a list of two colour indices. Thus, the i-th particle carries the following pair of indices

$$\begin{aligned} q(i) &\to (\texttt{colour1[i]}\,,\ 0) \\ \bar{q}(i) &\to (0\,,\ \texttt{colour2[i]}) \\ g(i) &\to (\texttt{colour1[i]}\,,\ \texttt{colour2[i]})\,. \end{aligned} \tag{4.18}$$

In Deductor, on the other hand, quarks, anti-quarks and gluons are represented by

$$\begin{aligned} q(i) &\to [\texttt{Q}\,,\ \texttt{next[i]}) \\ \bar{q}(i) &\to (\texttt{prev[i]}\,,\ \texttt{A}] \\ g(i) &\to (\texttt{prev[i]}\,,\ \texttt{next[i]})\,, \end{aligned} \tag{4.19}$$

where `Q` denotes the beginning and `A` the end of an open colour string. `prev[i]` refers to the particle index in the event, which is to the left of particle with index i. In the same way `next[i]` refers to the right partner on the colour string. The algorithm to translate colour flows into colour string configurations is

JHEP06(2015)033

1. Swap the flavour and the colour indices for initial state partons.

2. Enumerate all partons starting from -1, where -1 and 0 are reserved for the initial state partons. Colour-neutral particles are enumerated with numbers less than -1.

3. Iterate over all particles with index i applying

   (a) If (`colour1[i]`$\neq 0$ and `colour2[i]` $= 0$) then `prev[i]` $=$ `Q`.
   If (`colour1[i]`$= 0$ and `colour2[i]` $\neq 0$) then `next[i]` $=$ `A`.

   (b) Iterate over all particles with index $k \neq i$ applying
   If (`colour1[i]`$\neq 0$ and `colour1[i]`$=$ `colour2`[k]) then `next[i]`=k; `prev[k]`=i.

5 $t\bar{t}j$ production at the LHC with next-to-leading order matching

In this section, we present results for $pp \to t\bar{t}j + X$ production at next-to-leading order, obtained with HELAC-NLO, matched with the Nagy-Soper parton shower as implemented in DEDUCTOR. The NLO QCD corrections to the considered process have been previously computed in ref. [72–74]. Matching to a parton shower has been first considered in ref. [75, 76] using the POWHEG method [28, 30].

5.1 Setup

The results for $t\bar{t}j$ production are presented for pp collisions at the LHC with a center-of-mass energy of 8 TeV. The top quark is assumed to be stable and its mass is set to $m_t = 173.5\,\text{GeV}$, while the charm and bottom quarks are considered to be massless at fixed order. Results are obtained using the MSTW2008NLO PDF set [77] with five active flavours and the corresponding two-loop running of the strong coupling. We set the renormalization and factorization scales to the top quark mass, $\mu_R = \mu_F = m_t$, and the starting shower time to

$$e^{-t_0} = \min_{i \neq j} \left\{ \frac{2p_i \cdot p_j}{\mu_T^2 Q_0^2} \right\}, \tag{5.1}$$

where p_i and p_j are external momenta, Q_0 is the total final state momentum and $\mu_T = 1$ for the central prediction as explained below. Partons with pseudorapidity $|\eta| < 5$ are clustered using the anti-k_T jet algorithm [78], with the separation parameter $R = 1$. The resulting jets are sorted in decreasing order of p_T. We require the tagged jets to have transverse momentum of $p_T > 50\,\text{GeV}$ and rapidity in the range of $|y| < 5$.

We restrict our analysis to the perturbative parton shower evolution. Decays of unstable particles, hadronization and multiple interactions are not taken into account. The parton shower treats the charm and bottom as massive particles with masses $m_c = 1.4\,\text{GeV}$ and $m_b = 4.75\,\text{GeV}$. We provide the MSTW2008NLO PDF set at $\mu_F = 1$ GeV as the starting point for the evolution in DEDUCTOR. We also use the corresponding two-loop running of α_s, and restrict the parton shower to the leading colour approximation. Therefore, results presented in this section are accurate up to $\mathcal{O}(1/N_c^2)$.

In order to address the theoretical uncertainties, we investigate the scale dependence of cross sections and distributions on the unphysical scales μ_R, μ_F and the rescaling parameter μ_T. Here, μ_R is varied simultaneously with μ_F between $\mu_{R,F} = m_t/2$ and $\mu_{R,F} = 2m_t$.

JHEP06(2015)033

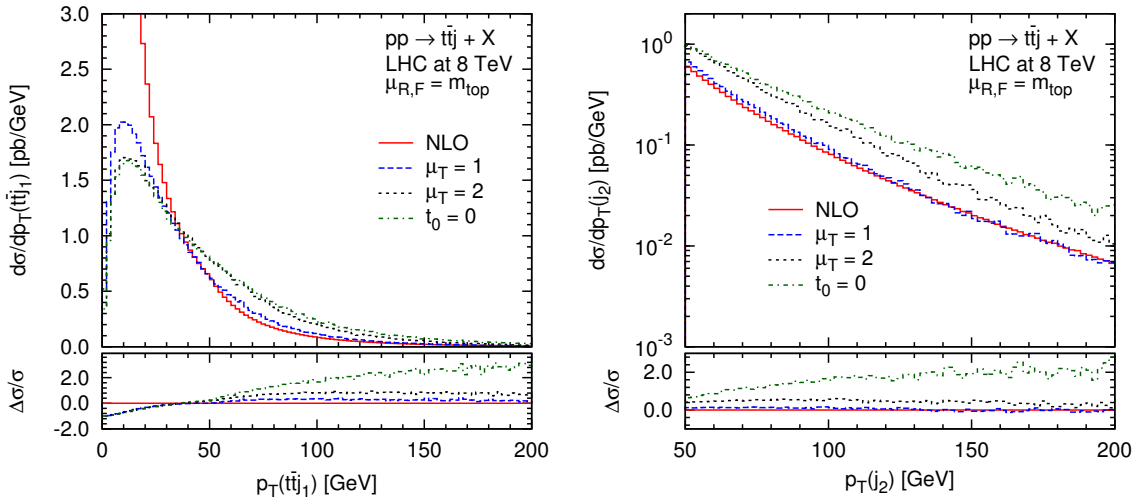

Figure 10. Differential cross section distributions as a function of the transverse momentum of the $t\bar{t}j_1$ system (left panel) and of the second hardest jet (right panel) for $pp \to t\bar{t}j + X$ at the LHC with $\sqrt{s} = 8\,\text{TeV}$. Comparison between the NLO result obtained with HELAC-NLO and the results produced by matching NLO predictions to DEDUCTOR for three different choices of the starting time. The scale choice is $\mu_F = \mu_R = m_t$. The lower panels display the relative deviation from the fixed order result. Notice, that $t_0 = 0$ corresponds to unrestricted shower radiation without relation to the kinematics of the underlying event. This choice should not be used in practice and it is shown for illustration purposes only.

On the other hand, both the central value of μ_T, μ_{T0}, and its variation range require a more thorough discussion, because this parameter is specific to the Nagy-Soper parton shower. Guidelines for a suitable choice of t_0 have already been presented in section 3.5. In practice, we consider exclusive distributions, which are especially sensitive to the parton shower effects, e.g. the transverse momentum, p_T, spectrum of the $t\bar{t}j_1$ system or of the second jet, j_2, which are equivalent at NLO. For large p_T values, the fixed order prediction is reliable and we would not like the shower to introduce substantial shape differences there. This can be achieved by a suitable choice of μ_{T0} as shown in figure 10, where the lower panel shows the relative deviation from the fixed order result defined as

$$\frac{\Delta\sigma}{\sigma} \equiv \frac{\sigma^{\text{NLO+PS}} - \sigma^{\text{NLO}}}{\sigma^{\text{NLO}}}\,. \tag{5.2}$$

The p_T spectra of $t\bar{t}j_1$ and j_2 coincide at NLO because of momentum conservation. After including shower effects, they deviate since the $t\bar{t}j_1$ system recoils against several jets. In addition, the parton shower generates corrections to the structure of the second jet. We can see that for $t_0 = 0$ and $\mu_T = 2$ the parton shower overshoots the tail of the transverse momentum spectra. The large higher order corrections can be explained by the exponentiation of non-singular emissions, as already reported in ref. [57] in the case of Higgs production. Decreasing the value of μ_T helps to recover the NLO predictions. We conclude that an appropriate choice of the central value of the starting time rescaling parameter is

$$\mu_{T0} = 1\,. \tag{5.3}$$

JHEP06(2015)033

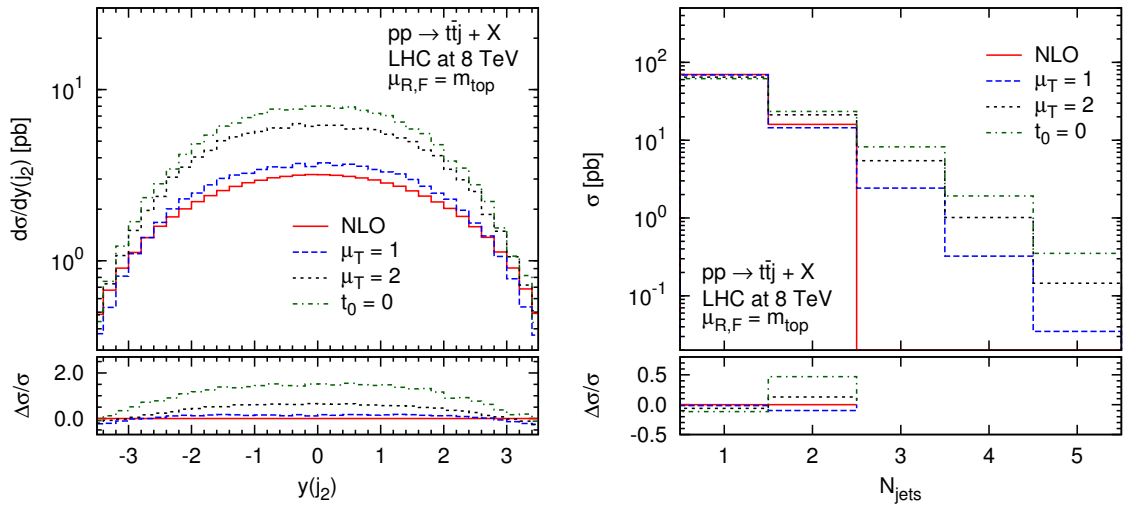

Figure 11. Differential cross section distribution as a function of the rapidity of the second hardest jet (left panel) and inclusive jet cross sections (right panel) for $pp \to t\bar{t}j + X$ at the LHC with $\sqrt{s} = 8\,\text{TeV}$. Comparison between the NLO result obtained with HELAC-NLO and the results produced by matching NLO predictions to DEDUCTOR for three different choices of the starting time. The scale choice is $\mu_F = \mu_R = m_t$. The lower panels display the relative deviation from the fixed order result.

We expect that the choice of μ_T will affect all exclusive distributions. We present two examples in figure 11: the rapidity of the second jet, $y(j_2)$, and the number of hard jets. Finally, after fixing the central value of μ_T, we choose to vary it between $\mu_T = \mu_{T0}/2$ and $\mu_T = 2\mu_{T0}$. This initial time variation is the dimensionless analogue of the resummation scale variation originally introduced in refs. [79–83] and first used in the context of event generators in ref. [84].

5.2 Results

The fixed order cross section at NLO obtained from the HELAC-NLO framework, including the theoretical error estimated via scale variation, reads

$$\sigma^{\text{NLO}}_{pp\to t\bar{t}j+X} = 86.04^{\,+5.10\ (\,+6\%)}_{-11.41\ (-13\%)}\ \text{pb}\,. \tag{5.4}$$

In order to obtain a reliable result including showering effects, we study the dependence of the cross section on the generation cut, denoted by p_T^{cut}. Table 1 contains values obtained at $\mu_F = \mu_R = m_t$ and $\mu_T = 1$. We see that for all values of p_T^{cut} but the last one, for which the generation cut is equal to the analysis cut, the total cross section is compatible with the fixed order prediction. For the following study, we choose a generation cut of $p_T(j_1) > 30\,\text{GeV}$. Varying the renormalization/factorization scale between $m_t/2 \le \mu_{R,F} \le 2m_t$ and the initial shower time rescaling parameter between $1/2 \le \mu_T \le 2$, the total cross section, together with its uncertainties, obtained after applying the parton shower is

$$\sigma^{\text{NLO+PS}}_{pp\to t\bar{t}j+X} = 86.11^{\,+4.38\ (\,+5\%)}_{-10.88\ (-13\%)}\ [\text{scales}]\ ^{+0.80\ (+1\%)}_{+2.17\ (+3\%)}\ [\text{PS time}]\ \text{pb}\,, \tag{5.5}$$

JHEP06(2015)033

$p_T^{\rm cut}$ [GeV]	$\sigma^{\rm NLO+PS}_{pp\to t\bar{t}j+X}$ [pb]	ϵ [‰]
5	86.51 ± 0.21	2.4
10	86.26 ± 0.17	2.0
15	86.22 ± 0.14	1.6
30	86.11 ± 0.13	1.5
40	86.01 ± 0.08	0.9
50	84.58 ± 0.07	0.8

Table 1. Total cross section for $pp \to t\bar{t}j+X$ at the LHC with $\sqrt{s} = 8\,\text{TeV}$, together with statistical and relative errors, for different values of the generation cut. Results are produced by matching HELAC-NLO predictions to DEDUCTOR. The cross section is calculated for $\mu_F = \mu_R = m_t$ and $\mu_T = 1$.

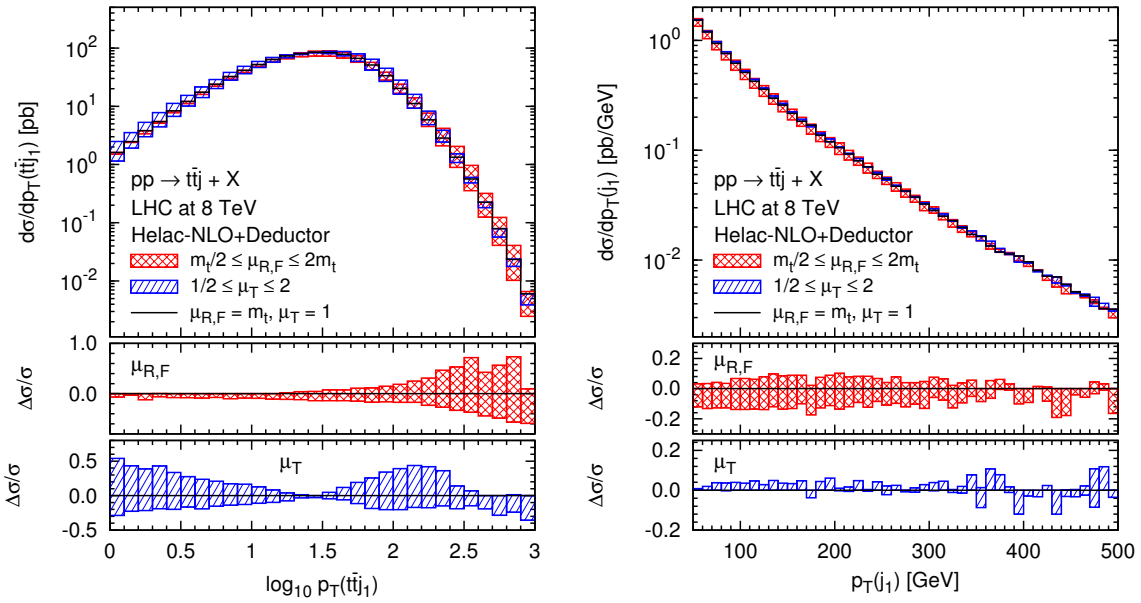

Figure 12. Differential cross section distributions as a function of the transverse momentum of the $t\bar{t}j_1$ system (left panel) and of the hardest jet (right panel) for $pp \to t\bar{t}j + X$ at the LHC with $\sqrt{s} = 8\,\text{TeV}$. Results are produced by matching HELAC-NLO predictions to DEDUCTOR. The uncertainty bands depict scale and initial shower time variation. The lower panels display the corresponding relative deviation from the central value, separately for $\mu_{R,F}$ and μ_T.

where the upper, (lower) values are given for $\mu_{R,F} = m_t/2$ $(2m_t)$ and $\mu_T = 1/2$ (2). The scale dependence of the total cross section, taken very conservatively as a maximum of the upper and lower results, is 13% or 9% after symmetrization. The dependence on the initial shower time is, by comparison, negligible. The situation is quite different when it comes to differential distributions as can be observed in figures 12 and 13, where the transverse momentum of the $t\bar{t}j_1$ system, the first and second hard jets together with inclusive jet cross sections are given. The variation bands for $\mu_{R,F}$ and μ_T in figures 12 and 13 have been obtained using the following sets of three parameter values: $\mu_{R,F} = \{m_t/2, m_t, 2m_t\}$ and

JHEP06(2015)033

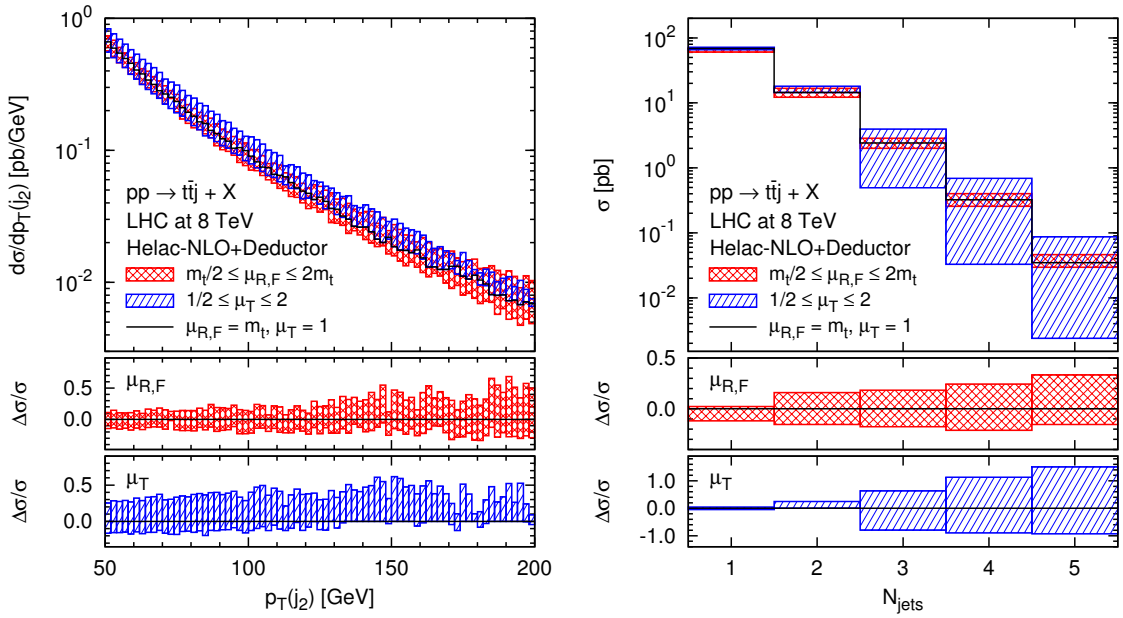

Figure 13. Differential cross section distribution as a function of the transverse momentum of the second jet (left panel) and inclusive jet cross sections (right panel) for $pp \to t\bar{t}j + X$ at the LHC with $\sqrt{s} = 8\,\text{TeV}$. Results are produced by matching HELAC-NLO predictions to DEDUCTOR. The uncertainty bands depict scale and initial shower time variation. The lower panels display the corresponding relative deviation from the central value, separately for $\mu_{R,F}$ and μ_T.

$\mu_T = \{1/2,\ 1,\ 2\}$, respectively. The lower panels of figures 12 and 13 display corresponding relative deviations from the central value, separately for $\mu_{R,F}$ and μ_T.

We start the discussion with the transverse momentum of the $p_T(t\bar{t}j_1)$ system, which is presented in figure 12 (left panel). At leading order, this observable is zero due to momentum conservation. When real emission contributions at the NLO level are included, this observable diverges as the transverse momentum of the entire system goes to zero. Therefore, it can only be reliably described by the fixed order calculation in the high p_T region. However, including the parton shower, the low p_T behavior is altered strongly by the Sudakov form factor as can be seen in figure 12. Indeed, for low values of the transverse momentum, the distribution is generated mostly by the parton shower. The reason is that the real radiation contribution, which is responsible for the divergent behaviour at fixed order receives subtractions, which match the singular behaviour for $p_T \to 0$. These subtractions belong to the same bin as the real radiation events themselves, contrary to the fixed order calculation, where they belong to the zero bin. Thus, the subtracted real radiation sample has low weight contributions for low p_T. In consequence, we observe a moderate dependence on μ_T in this region, which reaches factors of 1.5 at the lower end of the spectrum. This dependence decreases down to just a few percent around 30 GeV, whereas for moderate values of $p_T(t\bar{t}j_1)$ it is at the level of 20%–45%. The presence of a minimum dependence on μ_T is due to a crossing of the distribution for $\mu_T = 1/2$, which dominates at low p_T with the distribution for $\mu_T = 2$, which dominates at high p_T. The

JHEP06(2015)033

reason for a larger cross section for low values of μ_T and p_T is that the parton shower generates low p_T radiation only barely shifting events with zero p_T to non-zero values. On the other hand, high μ_T results in radiation of high p_T partons, which shift events to high p_T values. The situation is reversed when it comes to the renormalization and factorization scale dependence. Here, visible deviations from the central value occur once the matrix element is present. They grow substantially up to almost 80% at the end of the spectrum. This can be explained by the fact that the variation of $\mu_{R,F}$ is only implemented in the matrix element, while the shower does not depend directly on those scales but rather on t_0.

The $p_T(j_1)$ distribution of the hardest jet, which is given in figure 12 (right panel) shows a rather constant and small dependence on both parameters, $\mu_{R/F}$ and μ_T, as it has NLO accuracy. The $p_T(j_2)$ distribution of the second jet, which is presented in figure 13 (left panel), also shows a rather constant scale dependence with a somewhat larger variation range, as it is only LO accurate.

Finally, inclusive jet cross sections are shown in figure 13 (right panel). As expected, the NLO cross section with exactly one jet, which is given in the first bin, is rather insensitive to μ_T. Its theoretical error is at the 12% level. The μ_T dependence is slightly larger in the second bin, where the two jet cross section, correct only at the LO level, is stored. Also here, the theoretical error increases up to 16%. Starting from the third bin, cross sections are described via the shower evolution alone, therefore, fairly large variations can be noticed for both parameters, μ_T and $\mu_{R,F}$. For example, the scale dependence for the cross section with five jets is found to be around 35%. In addition, cross sections for higher multiplicities are severely affected by the cutoff on the parton shower emission phase space. This strong dependence can be partially cured when matrix elements for higher multiplicities are merged together and matched to the shower evolution as described e.g. in refs. [62, 85] for the LO and in refs. [64, 86] for the NLO case.

5.3 Comparison with other Monte Carlo event generators

In this section we compare our implementation of the NLO matching to the Nagy-Soper parton shower from Deductor, as implemented in Helac-Dipoles, with other matching procedures and shower programs. To be more specific, we use:

1. the Powheg-Box [30] implementation of $pp \to t\bar{t}j + X$ [76] in conjunction with the Pythia 8.1 [45] Monte Carlo program version 8.183, with the transverse-momentum ordered shower (dubbed Powheg+Pythia8),

2. the automatic solution of aMc@Nlo [59] including Pythia 6.4 [44] (version 6.428) with the virtuality-ordered or mass-ordered shower (dubbed aMc@Nlo+Pythia6Q),

3. the automatic solution of aMc@Nlo together with Pythia 8.1, once more with the transverse-momentum ordered shower (dubbed aMc@Nlo+Pythia8).

Once again, we do not include top quark decays, hadronization and multiple interactions. Thus, we are only comparing the perturbative evolution of different parton showers. In each case the default setup of the programs is used.

JHEP06(2015)033

The total cross sections together with their theoretical errors are

$$\sigma^{\text{NLO+PS}}_{pp\to t\bar{t}j+X}(\text{aMc@Nlo+Pythia6Q}) = 84.85^{\ +8.95\ (+11\%)}_{-13.75\ (-16\%)}\ [\text{scales}]\ \text{pb}\,, \tag{5.6}$$

$$\sigma^{\text{NLO+PS}}_{pp\to t\bar{t}j+X}(\text{aMc@Nlo+Pythia8}) = 89.55^{\ +8.44\ (\ +9\%)}_{-15.41\ (-17\%)}\ [\text{scales}]\ \text{pb}\,, \tag{5.7}$$

$$\sigma^{\text{NLO+PS}}_{pp\to t\bar{t}j+X}(\text{Powheg+Pythia8}) = 89.12^{+26.22\ (+29\%)}_{-8.96\ (-10\%)}\ [\text{scales}]\ \text{pb}\,. \tag{5.8}$$

We observe that all three calculations, although based on different shower ordering variables, give compatible results and agree within 4% with the Helac-Nlo+Deductor result from eq. (5.5). We note that, in case of Pythia8, the central prediction for our process is larger. Moreover, the scale dependence after symmetrization is below 13% for all cases but the Powheg+Pythia8, where it is slightly larger i.e. of the order of 20%.

In the next step, we extend our comparison to differential distributions and start with observables that are rather insensitive to parton shower effects. In figure 14, the transverse momentum and rapidity distributions of the top quark and the first jet are presented. For each observable the NLO result obtained with Helac-Nlo is plotted together with results produced by matching various NLO predictions to different parton showers. The lower panels display the relative deviation from the next-to-leading order result. All parton showers reproduce the corresponding NLO result correctly, and slight deviations from the fixed order calculation can only be seen in the tails of the distributions due to smaller statistics.

The same conclusions can be drawn from figure 15, where we show the invariant mass of the $t\bar{t}$ pair and the angular separation in the rapidity-azimuthal angle plane between the top and the anti-top quark

$$\Delta R_{ij} = \sqrt{(y_i - y_j)^2 + (\phi_i - \phi_j)^2}\,. \tag{5.9}$$

Overall, we observe that results obtained within the Helac-Nlo+Deductor framework are consistent with those of the other Monte-Carlo event generators used in this study. Let us emphasize, that not only various showers but also different matching schemes with distinct systematic uncertainties are examined here.

To assess potential differences among showers and matching procedures used in our analysis, we turn to observables, which are sensitive to the initial conditions of the parton evolution. As an example, we present in figure 16 the differential cross section distribution as a function of the transverse momentum of the $t\bar{t}j_1$ system. For clarity we give both a linear-scale (left panel) and a log-scale (right panel) version of the plot. We observe that the matching with Pythia8 yields similar results for both Mc@Nlo and Powheg, i.e. the hardest spectra and a lack of agreement with the fixed order prediction in the region where hard, well separated partons are produced. We have found discrepances even up to 120%. This suggests, that for the process at hand, initial condition of the transverse-momentum ordered shower from Pythia8 should be adjusted to restrict further the shower phase space where emissions become hard. On the other hand, aMc@Nlo+Pythia6Q nicely reproduces the NLO differential cross section in the high p_T region. We also note that it produces a softer spectrum. As for the Helac-Nlo+Deductor case, as already

JHEP06(2015)033

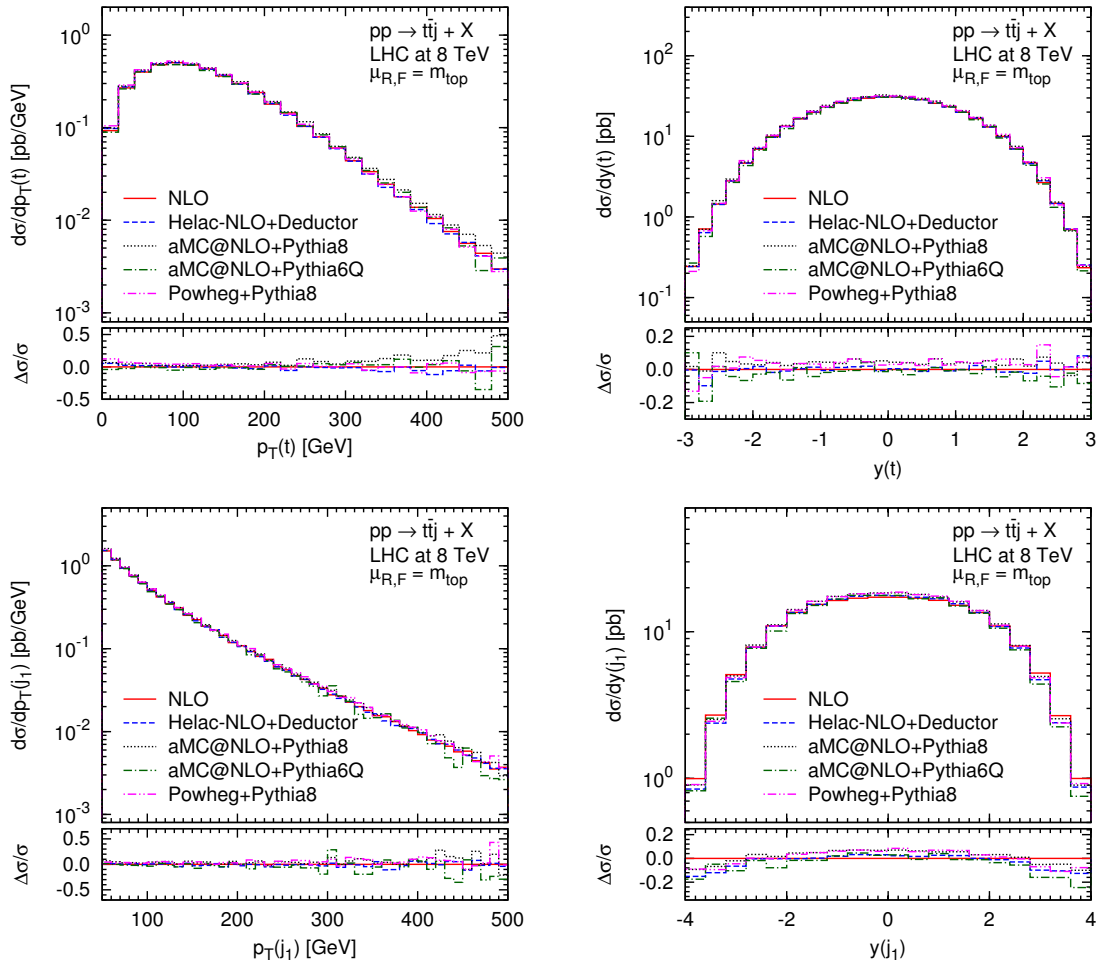

Figure 14. Differential cross section distributions as a function of the transverse momentum of the top quark (left upper panel) and of the first jet (left lower panel) as well as the rapidity of the top quark (right upper panel) and of the first jet (right lower panel) for $pp \to t\bar{t}j + X$ at the LHC with $\sqrt{s} = 8\,\text{TeV}$. Comparison between the NLO result obtained with HELAC-NLO and results produced by matching various NLO predictions to different parton showers. The scale choice is $\mu_F = \mu_R = m_t$. The lower panels display the relative deviation from the fixed order result.

explained, the parameter t_0 was chosen to preserve the NLO shape in the tail of the p_T spectrum of the $t\bar{t}j_1$ system.

In figure 17, the kinematics of the second jet is analysed. To be more precise, distributions in the transverse momentum and in rapidity are given. There is a good agreement between the spectra of aMC@NLO+PYTHIA6Q and HELAC-NLO+DEDUCTOR, with a somewhat narrower rapidity spectrum in the case of HELAC-NLO+DEDUCTOR. For aMC@NLO+PYTHIA8 and POWHEG+PYTHIA8, a difference in normalization can be observed, but the differential K-factor remains flat. This can be explained by larger emission rates that increase the amount of radiation.

In figure 18, the differential cross section as a function of the transverse momentum of the $t\bar{t}$ pair is presented. We observe a good agreement among all programs for $p_T >$

JHEP06(2015)033

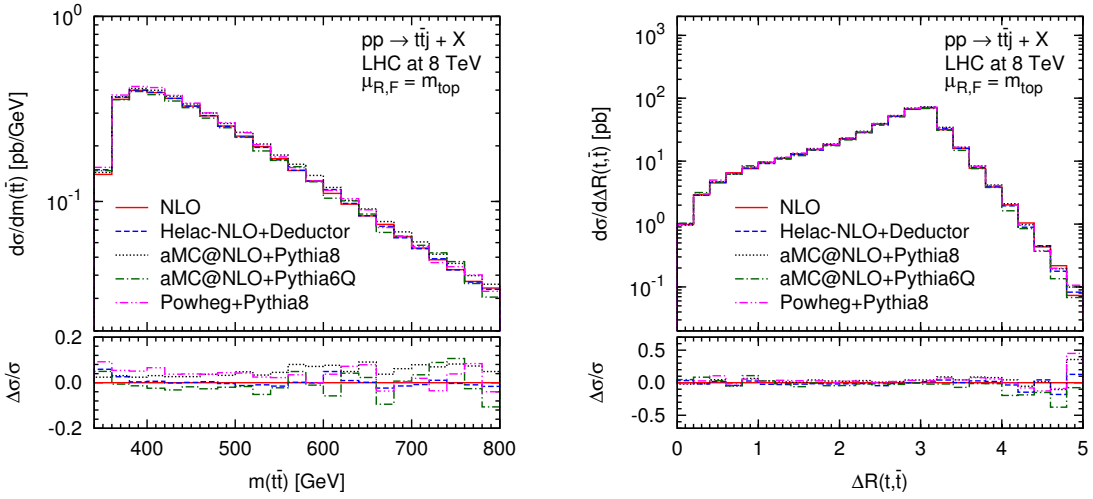

Figure 15. Differential cross section distributions as a function of the invariant mass of the $t\bar{t}$ pair (left panel) and of the $\Delta R_{t\bar{t}}$ (right panel) for $pp \to t\bar{t}j + X$ at the LHC with $\sqrt{s} = 8\,\text{TeV}$. Comparison between the NLO result obtained with HELAC-NLO and results produced by matching various NLO predictions to different parton showers. The scale choice is $\mu_F = \mu_R = m_t$. The lower panels display the relative deviation from the fixed order result.

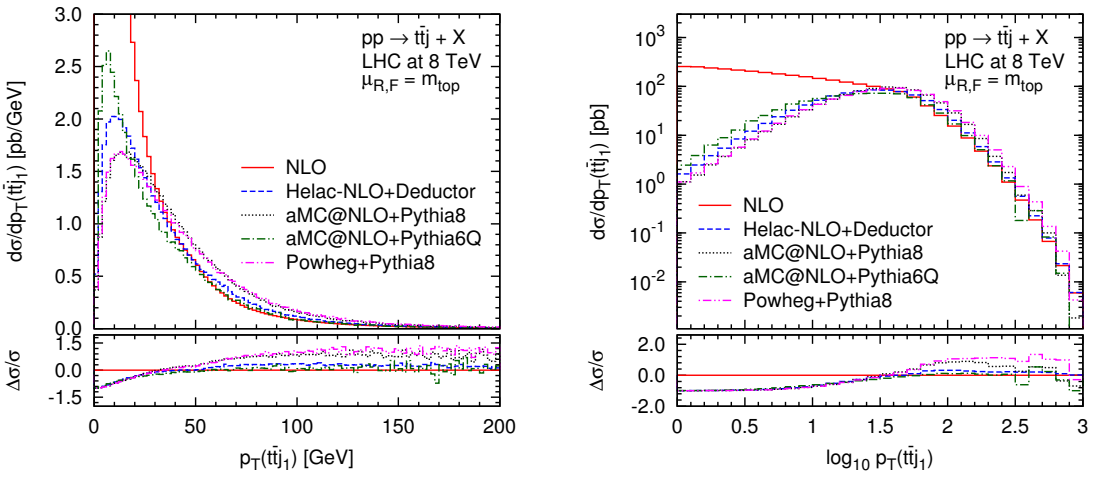

Figure 16. Differential cross section distributions as a function of the transverse momentum of the $t\bar{t}j_1$ system for $pp \to t\bar{t}j + X$ at the LHC with $\sqrt{s} = 8\,\text{TeV}$. Comparison between the NLO result obtained with HELAC-NLO and results produced by matching various NLO predictions to different parton showers. The scale choice is $\mu_F = \mu_R = m_t$. The lower panels display the relative deviation from the fixed order result.

50 GeV i.e. above the analysis cut. Below this value the prediction is only leading order accurate and thus strongly depends on the initial shower conditions. Also shown in figure 18 are inclusive jet cross sections. In the first (second) bin the exclusive cross section is accurate at next-to-leading order (leading order). Starting from the third bin on, cross sections are only described with leading-logarithmic accuracy via the parton shower alone. Results for exclusive cross sections with $N_{\text{jets}} = 1$ and $N_{\text{jets}} = 2$ are in agreement with our

JHEP06(2015)033

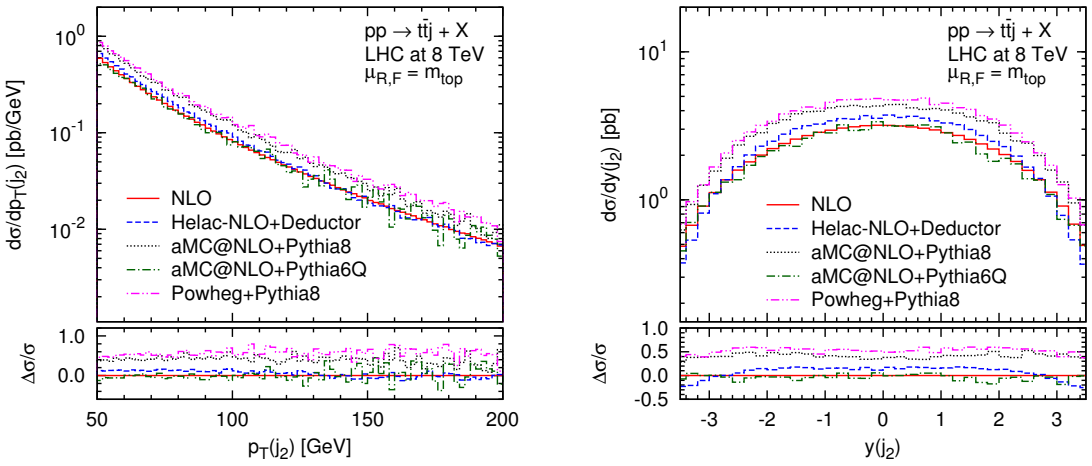

Figure 17. Differential cross section distributions as a function of the the transverse momentum (left panel) and rapidity of the second jet (left panel) for $pp \to t\bar{t}j + X$ at the LHC with $\sqrt{s} = 8\,\text{TeV}$. Comparison between the NLO result obtained with HELAC-NLO and results produced by matching various NLO predictions to different parton showers. The scale choice is $\mu_F = \mu_R = m_t$. The lower panels display the relative deviation from the fixed order result.

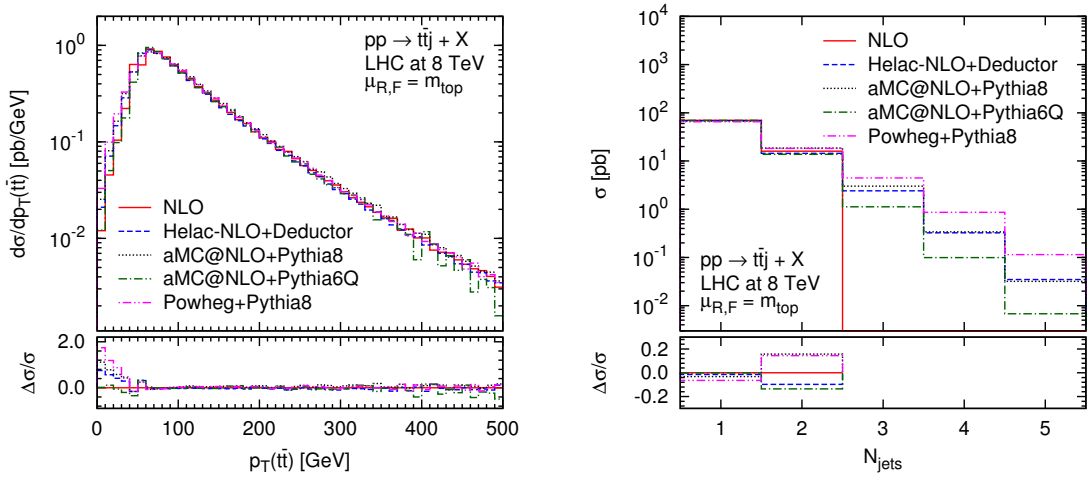

Figure 18. Differential cross section distribution as a function of the transverse momentum of the $t\bar{t}$ pair (left panel) and inclusive jet cross sections (right panel) for $pp \to t\bar{t}j + X$ at the LHC with $\sqrt{s} = 8\,\text{TeV}$. Comparison between the NLO result obtained with HELAC-NLO and results produced by matching various NLO predictions to different parton showers. The scale choice is $\mu_F = \mu_R = m_t$. The lower panels display the relative deviation from the fixed order result.

observations for other observables. The picture is vastly different for all showers, however, when $N_{\text{jets}} \geq 3$. In this case, the POWHEG+PYTHIA8 framework (aMC@NLO+PYTHIA6Q) produces the highest (lowest) number of hard jets.

Finally, cross sections (in fb) for inclusive $\sigma(t\bar{t} + n \text{ jets})$ rates are presented in table 2. Table 3 contains cross section ratios, i.e. $\sigma(t\bar{t} + n + 1 \text{ jets})/\sigma(t\bar{t} + n \text{ jets})$.

JHEP06(2015)033

Framework	$\sigma^{[\geq 1 \text{ jet}]}$	$\sigma^{[\geq 2 \text{ jets}]}$	$\sigma^{[\geq 3 \text{ jets}]}$	$\sigma^{[\geq 4 \text{ jets}]}$	$\sigma^{[\geq 5 \text{ jets}]}$
Helac-Nlo+Deductor	86110	17204	2780	362	38
aMc@Nlo+Pythia6Q	84850	15030	1230	106	7
aMc@Nlo+Pythia8	89556	21872	3377	372	32
Powheg+Pythia8	89121	23744	5458	992	129

Table 2. Cross sections (in fb) for the inclusive jet rates at the LHC with $\sqrt{s} = 8\,\text{TeV}$, according to the default settings of the various codes.

Framework	$\sigma^{[\geq 2]}/\sigma^{[\geq 1]}$	$\sigma^{[\geq 3]}/\sigma^{[\geq 2]}$	$\sigma^{[\geq 4]}/\sigma^{[\geq 3]}$	$\sigma^{[\geq 5]}/\sigma^{[\geq 4]}$
Helac-Nlo+Deductor	0.20	0.16	0.13	0.10
aMc@Nlo+Pythia6Q	0.18	0.08	0.09	0.07
aMc@Nlo+Pythia8	0.24	0.15	0.11	0.09
Powheg+Pythia8	0.27	0.23	0.18	0.13

Table 3. Cross section ratios for $(n+1)/n$ inclusive jet rates at the LHC with $\sqrt{s} = 8\,\text{TeV}$, according to the default settings of the various codes.

6 Conclusions

In this publication, we have presented a next-to-leading order matching scheme for the Nagy-Soper parton shower. We based our construction on the original Mc@Nlo approach. Besides the general formulation, we have performed real simulations for top-quark pair production in association with a jet at the LHC, using an implementation within the framework of the public codes Helac-Nlo and Deductor.

Our general conclusion is that the combination Helac-Nlo+Deductor is able to provide results for non-trivial processes, which remain in reasonable agreement with other Monte Carlo systems. Indeed, for observables, which are rather insensitive to showering effects, the differential cross sections are in very good agreement between different programs and the fixed order NLO calculation. Inevitable differences for infrared sensitive observables, on the other hand, seem to be justifiable in size in the sense that all predictions have overlapping uncertainty bands. Of course, further studies are needed here.

We note that our simulations are at the same level of logarithmic precision as those of others. For now, we are only correct as far as the leading behaviour is concerned. Future developments in Deductor will allow us to include soft-gluon intereference effects yielding next-to-leading logarithmic accuracy. This step still requires some improvements of our implementation in Helac-Dipoles. In particular, it will be necessary to transfer colour-configuration information exactly, as opposed to the current leading-colour approximation. We leave this to future work.

Finally, we expect that the Nagy-Soper parton shower will open new opportunities for understanding parton shower systematics for processes with non-trivial colour exchange. Here, the road is still long, as we must remember that, ultimately, hadronization models must be included. The latter, however, require tuning to the shower. There are also interesting problems in merging different multiplicity samples generated by our software.

JHEP06(2015)033

Acknowledgments

We would like to thank M. Krämer and Z. Nagy for discussions at preliminary stages of this study. The work of M. Czakon and H. Hartanto was supported by the German Research Foundation (DFG) via the Sonderforschungsbereich/Transregio SFB/TR-9 "Computational Particle Physics". M. Worek and M. Kraus acknowledge support by the DFG under Grant No. WO 1900/1-1 ("Signals and Backgrounds Beyond Leading Order. Phenomenological studies for the LHC"). In addition, this research was supported in part by the Research Funding Program ARISTEIA, HOCTools (co-financed by the European Union (European Social Fund ESF) and Greek national funds through the Operational Program "Education and Lifelong Learning" of the National Strategic Reference Framework (NSRF)).

A Simplified matching scheme

In this appendix, we discuss the simplified matching prescription that we have implemented starting from spin and colour averaged amplitudes. We also prove that it yields NLO accuracy at leading colour, as long as the observable is not sensitive to spin correlations. The simplifications match the current DEDUCTOR functionality and relate to a spin and colour averaged quantum density

$$|\rho) = \sum_m \frac{1}{m!} \int [d\{p,f\}_m] |\{p,f\}_m)(\{p,f\}_m|\rho)\,, \tag{A.1}$$

where

$$(\{p,f\}_m|\rho) = \sum_{\{s\}_m,\{s'\}_m} \sum_{\{c\}_m,\{c'\}_m} \langle \{s,c\}_m|\{s',c'\}_m\rangle\, \rho(\{p,f,s',c',s,c\}_m)\,. \tag{A.2}$$

Averaging over spin and colour reduces tremendously the complexity of the calculation. However, the parton shower requires a colour configuration for each phase space point $\{p,f\}_m$ in order to perform the evolution. Starting from colour averaged weights $(\{p,f\}_m|\rho)$ one can recover leading colour correlations, $(\{p,f,c\}_m|\rho)$, by including a colour weight $C_w(\{p,f,c\}_m)$, defined by

$$C_w(\{p,f,c\}_m) = \frac{(\{p,f,c\}_m|\rho_m^{(0)})}{\sum_{\{\hat{c}\}_m}(\{p,f,\hat{c}\}_m|\rho_m^{(0)})}\,. \tag{A.3}$$

The simplified matching prescription accounting for generation cuts is then

$$\begin{aligned}
\sigma[F] = &\int \frac{[d\{p,f,c\}_m]}{m!} (F|\mathrm{U}(t_F,t_0)|\{p,f,c\}_m) C_w(\{p,f,c\}_m)(\{p,f\}_m|\Omega|\rho_m^{(0)}) F_I(\{p,f\}_m) \\
&+ \int \frac{[d\{p,f,c\}_{m+1}]}{(m+1)!} (F|\mathrm{U}(t_F,t_0)|\{p,f,c\}_{m+1}) C_w(\{p,f,c\}_{m+1}) \\
&\quad \times (\{p,f\}_{m+1}|R) F_I(\{p,f\}_{m+1}) \\
&\equiv \sigma_m[F] + \sigma_{m+1}[F]\,,
\end{aligned} \tag{A.4}$$

where the action of the operator Ω is given by

$$(\{p,f\}_m|\Omega|\rho_m^{(0)}) = \omega(\{p,f\}_m)(\{p,f\}_m|\rho_m^{(0)})\,, \tag{A.5}$$

with

$$\omega(\{p,f\}_m) = 1 + \frac{(\{p,f\}_m|\rho_m^{(1)})}{(\{p,f\}_m|\rho_m^{(0)})} + \frac{(\{p,f\}_m|\mathbf{I}(t_0)+\mathbf{K}(t_0)+\mathbf{P}|\rho_m^{(0)})}{(\{p,f\}_m|\rho_m^{(0)})}\,. \tag{A.6}$$

The density matrix for the real subtracted cross section, $(\{p,f\}_{m+1}|R)$, is defined as

$$\begin{aligned}(\{p,f\}_{m+1}|R) \equiv (\{p,f\}_{m+1}|\rho_{m+1}^{(0)}) - \int_{t_0}^{\infty} d\tau \sum_{\{s,s',c,c'\}} \langle\{s',c'\}_{m+1}|\{s,c\}_{m+1}\rangle \\ \times \int \frac{[d\{\hat{p},\hat{f},\hat{s}',\hat{c}',\hat{s},\hat{c}\}_m]}{m!}(\{\hat{p},\hat{f},\hat{s}',\hat{c}',\hat{s},\hat{c}\}_m|\rho_m^{(0)})\; F_I(\{\hat{p},\hat{f}\}_m) \\ \times (\{p,f,s',c',s,c\}_{m+1}|\mathcal{H}_I(\tau)|\{\hat{p},\hat{f},\hat{s}',\hat{c}',\hat{s},\hat{c}\}_m)\,,\end{aligned} \tag{A.7}$$

where we specified explicitly the full quantum correlations in the subtraction terms required for the removal of kinematic singularities. $\mathcal{H}_I(t)$ is the Nagy-Soper real splitting operator without any approximations. The inclusive jet functions $F_I(\{p,f\}_m)$ define the generation cuts.

Let us now study the accuracy of eq. (A.4) after expansion to next-to-leading order. The parton shower evolution operator, currently available in DEDUCTOR, reads

$$\mathrm{U}(t_F,t_0) = N^{\mathrm{LC+}}(t_F,t_0) + \int_{t_0}^{t_F} d\tau\; \mathrm{U}(t_F,\tau)\overline{\mathcal{H}}_I^{\mathrm{LC+}}(\tau)N^{\mathrm{LC+}}(\tau,t_0)\,, \tag{A.8}$$

where $\overline{\mathcal{H}}_I^{\mathrm{LC+}}(\tau)$ denotes the spin averaged splitting operator in the LC+ approximation and $N^{\mathrm{LC+}}(t_F,t_0)$ the corresponding Sudakov form factor, as discussed in section 2.6. Inserting eq. (A.8) in $\sigma_m[F]$ and expanding the evolution yields

$$\begin{aligned}\sigma_m[F] = \frac{1}{m!}\int [d\{p,f,c\}_m](F|\{p,f,c\}_m)C_w(\{p,f,c\}_m)(\{p,f\}_m|\Omega|\rho_m^{(0)})F_I(\{p,f\}_m) \\ + \frac{1}{m!}\int [d\{p,f,c\}_m]\int_{t_0}^{t_F} d\tau\left(F|\overline{\mathcal{H}}_I^{\mathrm{LC+}}(\tau) - \mathcal{V}^{\mathrm{LC+}}(\tau)|\{p,f,c\}_m\right) \\ \times C_w(\{p,f,c\}_m)(\{p,f\}_m|\rho_m^{(0)})F_I(\{p,f\}_m) + \mathcal{O}(\alpha_s^2)\,.\end{aligned} \tag{A.9}$$

Using the approximations

$$\mathcal{V}(\tau) = \mathcal{V}^{\mathrm{LC+}}(\tau) + \mathcal{O}(1/N_c^2)\,, \tag{A.10}$$

and

$$C_w(\{p,f,c\}_m)(\{p,f\}_m|\rho_m^{(0,1)}) = (\{p,f,c\}_m|\rho_m^{(0,1)}) + \mathcal{O}(1/N_c^2)\,, \tag{A.11}$$

eq. (A.9) reduces to

$$\begin{aligned}\sigma_m[F] = \frac{1}{m!}\int [d\{p,f,c\}_m](F|\{p,f,c\}_m)(\{p,f,c\}_m|\left[|\rho_m^{(0)}) + |\rho_m^{(1)}) + \mathbf{P}|\rho_m^{(0)})\right]F_I(\{p,f\}_m) \\ + \frac{1}{m!}\int [d\{p,f,c\}_m]\int_{t_0}^{\infty} d\tau\;(F|\overline{\mathcal{H}}_I^{\mathrm{LC+}}(\tau)|\{p,f,c\}_m)(\{p,f,c\}_m|\rho_m^{(0)})F_I(\{p,f\}_m) \\ + \mathcal{O}(\alpha_s^2, 1/N_c^2, \Delta\sigma)\,.\end{aligned} \tag{A.12}$$

Here, $\Delta\sigma$ represents the error resulting from the limit $t_F \to \infty$.

JHEP06(2015)033

Let us now turn to the $\sigma_{m+1}[F]$. Expanding the shower evolution and making use of eq. (A.11) to recover the leading colour correlated real matrix element, we find

$$\begin{aligned}\sigma_{m+1}[F] = \int \frac{[d\{p,f,c\}_{m+1}]}{(m+1)!}(F|\{p,f,c\}_{m+1})F_I(\{p,f\}_{m+1})\Bigg[(\{p,f,c\}_{m+1}|\rho^{(0)}_{m+1}) \\ - \int_{t_0}^{\infty} d\tau \sum_{\{\bar{s},\bar{s}',\bar{c}',\bar{c}\}_{m+1}} \langle\{\bar{s}',\bar{c}'\}_{m+1}|\{\bar{s},\bar{c}\}_{m+1}\rangle\, C_w(\{p,f,c\}_{m+1}) \\ \times \int \frac{[d\{\hat{p},\hat{f},\hat{s}',\hat{c}',\hat{s},\hat{c}\}_m]}{m!}(\{\hat{p},\hat{f},\hat{s}',\hat{c}',\hat{s},\hat{c}\}_m|\rho^{(0)}_m)\; F_I(\{\hat{p},\hat{f}\}_m) \\ \times (\{p,f,\bar{s}',\bar{c}',\bar{s},\bar{c}\}_{m+1}|\mathcal{H}_I(\tau)|\{\hat{p},\hat{f},\hat{s}',\hat{c}',\hat{s},\hat{c}\}_m)\Bigg] + \mathcal{O}(\alpha_s^2, 1/N_c^2) \\ \equiv \sigma^R_{m+1}[F] - \sigma^S_{m+1}[F] + \mathcal{O}(\alpha_s^2, 1/N_c^2)\,.\end{aligned} \tag{A.13}$$

In the following we will focus on the subtraction terms $\sigma^S_{m+1}[F]$. The summation over $\{c\}_{m+1}$ can be eliminated by

$$\begin{aligned}\int [d\{p,f,c\}_{m+1}] C_w(\{p,f,c\}_{m+1})(F|\{p,f,c\}_{m+1}) \\ = \int [d\{p,f\}_{m+1}](F|\{p,f\}_{m+1}) + \mathcal{O}(1/N_c^2)\,.\end{aligned} \tag{A.14}$$

By a further approximation to the colour correlator

$$\langle\{\bar{c}'\}_{m+1}|\{\bar{c}\}_{m+1}\rangle = \langle\{\bar{c}\}_{m+1}|\{\bar{c}\}_{m+1}\rangle\, \delta\left(\{\bar{c}'\}_{m+1};\{\bar{c}\}_{m+1}\right) + \mathcal{O}(1/N_c^2)\,, \tag{A.15}$$

we recover leading colour correlations

$$\begin{aligned}\int [d\{p,f\}_{m+1}] \sum_{\{\bar{c}\}_{m+1}} (F|\{p,f\}_{m+1})\,\langle\{\bar{c}\}_{m+1}|\{\bar{c}\}_{m+1}\rangle \\ = \int [d\{p,f,\bar{c}\}_{m+1}](F|\{p,f,\bar{c}\}_{m+1})\,.\end{aligned} \tag{A.16}$$

In the following we rename $\bar{c} \to c$ and drop the second colour index in $(\{p,f,\bar{s}',c,\bar{s},c\}_{m+1}|$. In addition, we use

$$\mathcal{H}_I(\tau) = \mathcal{H}_I^{\mathrm{LC+}}(\tau) + \mathcal{O}(1/N_c^2)\,, \tag{A.17}$$

to obtain the following form for $\sigma^S_{m+1}[F]$

$$\begin{aligned}\sigma^S_{m+1}[F] = \frac{1}{(m+1)!m!}\int [d\{p,f,c\}_{m+1}][d\{\hat{p},\hat{f},\hat{s}',\hat{c}',\hat{s},\hat{c}\}_m]F_I(\{\hat{p},\hat{f}\}_m)F_I(\{p,f\}_{m+1}) \\ \times (F|\{p,f,c\}_{m+1}) \int_{t_0}^{\infty} d\tau \sum_{\{\bar{s},\bar{s}'\}_{m+1}} \langle\{\bar{s}'\}_{m+1}|\{\bar{s}\}_{m+1}\rangle\,(\{\hat{p},\hat{f},\hat{s}',\hat{c}',\hat{s},\hat{c}\}_m|\rho^{(0)}_m) \\ \times (\{p,f,\bar{s}',\bar{s},c\}_{m+1}|\mathcal{H}_I^{\mathrm{LC+}}(\tau)|\{\hat{p},\hat{f},\hat{s}',\hat{c}',\hat{s},\hat{c}\}_m) + \mathcal{O}(\alpha_s^2, 1/N_c^2)\,.\end{aligned} \tag{A.18}$$

It is now necessary to remove spin correlations. This can only be achieved, if $(F|\{p,f,c\}_{m+1})$ and $F_I(\{p,f\}_{m+1})$ are sufficiently inclusive to allow an azimuthal average. A typical case

JHEP06(2015)033

would be an observable with NLO accuracy, where the azimuthal average corresponds to the complete phase space integral over unresolved jets. On the example of top-quark pair production with at least one jet, this would be any observable insensitive to additional jets. Once an azimuthal average has been performed, spin correlations vanish as demonstrated in ref. [16] (chapter 12)

$$\begin{aligned}\int \frac{d\phi}{2\pi} \sum_{\{\bar{s},\bar{s}'\}_{m+1}} \langle\{\bar{s}'\}_{m+1}|\{\bar{s}\}_{m+1}\rangle \left(\{p,f,\bar{s}',\bar{s},c\}_{m+1}|\mathcal{H}_I^{\mathrm{LC+}}(\tau)|\{\hat{p},\hat{f},\hat{s}',\hat{c}',\hat{s},\hat{c}\}_m\right) \\ = \langle\{\hat{s}'\}_m|\{\hat{s}\}_m\rangle \left(\{p,f,c\}_{m+1}|\overline{\mathcal{H}}_I^{\mathrm{LC+}}(\tau)|\{\hat{p},\hat{f},\hat{c}',\hat{c}\}_m\right),\end{aligned} \tag{A.19}$$

which can be further transformed with

$$\begin{aligned}\left(\{p,f,c\}_{m+1}|\overline{\mathcal{H}}_I^{\mathrm{LC+}}(\tau)|\{\hat{p},\hat{f},\hat{c}',\hat{c}\}_m\right) = \left(\{p,f,c\}_{m+1}|\overline{\mathcal{H}}_I^{\mathrm{LC+}}(\tau)|\{\hat{p},\hat{f},\hat{c}\}_m\right) \\ \times \delta\left(\{\hat{c}'\}_m;\{\hat{c}\}_m\right) + \mathcal{O}(1/N_c^2)\,.\end{aligned} \tag{A.20}$$

Substituting eq. (A.19) and eq. (A.20) into eq. (A.18) we obtain

$$\begin{aligned}\sigma_{m+1}^S[F] = \frac{1}{(m+1)!m!}\int [d\{p,f,c\}_{m+1}][d\{\hat{p},\hat{f},\hat{c}\}_m](F|\{p,f,c\}_{m+1}) \\ \times \int_{t_0}^{\infty} d\tau(\{p,f,c\}_{m+1}|\overline{\mathcal{H}}_I^{\mathrm{LC+}}(\tau)|\{\hat{p},\hat{f},\hat{c}\}_m)F_I(\{\hat{p},\hat{f}\}_m)F_I(\{p,f\}_{m+1}) \\ \times \sum_{\{\hat{s},\hat{s}'\}_m} \langle\{\hat{s}'\}_m|\{\hat{s}\}_m\rangle\,(\{\hat{p},\hat{f},\hat{s}',\hat{s},\hat{c}\}_m|\rho_m^{(0)}) + \mathcal{O}(\alpha_s^2,1/N_c^2)\,.\end{aligned} \tag{A.21}$$

The last line of eq. (A.21) corresponds to the leading colour, spin averaged quantum density matrix

$$\sum_{\{\hat{s},\hat{s}'\}_m} \langle\{\hat{s}'\}_m|\{\hat{s}\}_m\rangle\,(\{\hat{p},\hat{f},\hat{s}',\hat{s},\hat{c}\}_m|\rho_m^{(0)}) = (\{\hat{p},\hat{f},\hat{c}\}_m|\rho_m^{(0)})\,. \tag{A.22}$$

With these approximations the final expression for $\sigma_{m+1}^S[F]$ reads

$$\begin{aligned}\sigma_{m+1}^S[F] = \frac{1}{(m+1)!m!}\int [d\{\hat{p},\hat{f},\hat{c}\}_{m+1}][d\{p,f,c\}_m]\int_{t_0}^{t_F} d\tau\ (F|\{\hat{p},\hat{f},\hat{c}\}_{m+1}) \\ \times F_I(\{\hat{p},\hat{f}\}_{m+1})\left(\{\hat{p},\hat{f},\hat{c}\}_{m+1}|\overline{\mathcal{H}}_I^{\mathrm{LC+}}(\tau)|\{p,f,c\}_m\right) \\ \times (\{p,f,c\}_m|\rho_m^{(0)})F_I(\{p,f\}_m) + \mathcal{O}(\alpha_s^2,1/N_c^2,\Delta\sigma)\,.\end{aligned} \tag{A.23}$$

Combining $\sigma_m[F]$ from eq. (A.12) with $\sigma_{m+1}^R[F]$ and $\sigma_{m+1}^S[F]$ from eqs. (A.13) and (A.23) yields

$$\begin{aligned}\sigma[F] &= \sigma_m[F] + \sigma_{m+1}^R[F] - \sigma_{m+1}^S[F] \\ &= \sigma^{\mathrm{LC-NLO}}[F] \\ &\quad + \frac{1}{(m+1)!m!}\int [d\{\hat{p},\hat{f},\hat{c}\}_{m+1}][d\{p,f,c\}_m]\int_{t_0}^{t_F} d\tau\ (F|\{\hat{p},\hat{f},\hat{c}\}_{m+1}) \\ &\quad \times (\{\hat{p},\hat{f},\hat{c}\}_{m+1}|\overline{\mathcal{H}}_I^{\mathrm{LC+}}(\tau)|\{p,f,c\}_m)(\{p,f,c\}_m|\rho_m^{(0)}) \\ &\quad \times F_I(\{p,f\}_m)\left[1 - F_I(\{\hat{p},\hat{f}\}_{m+1})\right] + \mathcal{O}(\alpha_s^2,1/N_c^2,\Delta\sigma)\,.\end{aligned} \tag{A.24}$$

The last term vanishes for suitable generation cuts as specified in section 3.3. In conclusion, we have shown that the simplified matching approach yields a prescription that is accurate at NLO to the level of leading colour.

JHEP06(2015)033

References

[1] G. Marchesini and B.R. Webber, *Simulation of QCD Jets Including Soft Gluon Interference*, *Nucl. Phys.* **B 238** (1984) 1 [INSPIRE].

[2] T. Sjöstrand, *A Model for Initial State Parton Showers*, *Phys. Lett.* **B 157** (1985) 321 [INSPIRE].

[3] M. Bengtsson, T. Sjöstrand and M. van Zijl, *Initial State Radiation Effects on W and Jet Production*, *Z. Phys.* **C 32** (1986) 67 [INSPIRE].

[4] M. Bengtsson and T. Sjöstrand, *A Comparative Study of Coherent and Noncoherent Parton Shower Evolution*, *Nucl. Phys.* **B 289** (1987) 810 [INSPIRE].

[5] G. Marchesini and B.R. Webber, *Monte Carlo Simulation of General Hard Processes with Coherent QCD Radiation*, *Nucl. Phys.* **B 310** (1988) 461 [INSPIRE].

[6] L. Lönnblad, *ARIADNE version 4: A program for simulation of QCD cascades implementing the color dipole model*, *Comput. Phys. Commun.* **71** (1992) 15 [INSPIRE].

[7] M. Dinsdale, M. Ternick and S. Weinzierl, *Parton showers from the dipole formalism*, *Phys. Rev.* **D 76** (2007) 094003 [arXiv:0709.1026] [INSPIRE].

[8] S. Schumann and F. Krauss, *A parton shower algorithm based on Catani-Seymour dipole factorisation*, *JHEP* **03** (2008) 038 [arXiv:0709.1027] [INSPIRE].

[9] S. Platzer and S. Gieseke, *Coherent Parton Showers with Local Recoils*, *JHEP* **01** (2011) 024 [arXiv:0909.5593] [INSPIRE].

[10] A. Gehrmann-De Ridder, M. Ritzmann and P.Z. Skands, *Timelike Dipole-Antenna Showers with Massive Fermions*, *Phys. Rev.* **D 85** (2012) 014013 [arXiv:1108.6172] [INSPIRE].

[11] S. Platzer and M. Sjodahl, *Subleading N_c improved Parton Showers*, *JHEP* **07** (2012) 042 [arXiv:1201.0260] [INSPIRE].

[12] M. Ritzmann, D.A. Kosower and P. Skands, *Antenna Showers with Hadronic Initial States*, *Phys. Lett.* **B 718** (2013) 1345 [arXiv:1210.6345] [INSPIRE].

[13] L. Hartgring, E. Laenen and P. Skands, *Antenna Showers with One-Loop Matrix Elements*, *JHEP* **10** (2013) 127 [arXiv:1303.4974] [INSPIRE].

[14] S. Catani and M.H. Seymour, *A General algorithm for calculating jet cross-sections in NLO QCD*, *Nucl. Phys.* **B 485** (1997) 291 [hep-ph/9605323] [INSPIRE].

[15] S. Catani, S. Dittmaier, M.H. Seymour and Z. Trócsányi, *The dipole formalism for next-to-leading order QCD calculations with massive partons*, *Nucl. Phys.* **B 627** (2002) 189 [hep-ph/0201036] [INSPIRE].

[16] Z. Nagy and D.E. Soper, *Parton showers with quantum interference*, *JHEP* **09** (2007) 114 [arXiv:0706.0017] [INSPIRE].

[17] Z. Nagy and D.E. Soper, *Parton showers with quantum interference: Leading color, spin averaged*, *JHEP* **03** (2008) 030 [arXiv:0801.1917] [INSPIRE].

JHEP06(2015)033

[18] Z. Nagy and D.E. Soper, *Parton showers with quantum interference: Leading color, with spin*, *JHEP* **07** (2008) 025 [arXiv:0805.0216] [INSPIRE].

[19] Z. Nagy and D.E. Soper, *On the transverse momentum in Z-boson production in a virtuality ordered parton shower*, *JHEP* **03** (2010) 097 [arXiv:0912.4534] [INSPIRE].

[20] Z. Nagy and D.E. Soper, *Final state dipole showers and the DGLAP equation*, *JHEP* **05** (2009) 088 [arXiv:0901.3587] [INSPIRE].

[21] Z. Nagy and D.E. Soper, *Parton shower evolution with subleading color*, *JHEP* **06** (2012) 044 [arXiv:1202.4496] [INSPIRE].

[22] Z. Nagy and D.E. Soper, *Ordering variable for parton showers*, *JHEP* **06** (2014) 178 [arXiv:1401.6366] [INSPIRE].

[23] Z. Nagy and D.E. Soper, *Parton distribution functions in the context of parton showers*, *JHEP* **06** (2014) 179 [arXiv:1401.6368] [INSPIRE].

[24] Z. Nagy and D.E. Soper, *A parton shower based on factorization of the quantum density matrix*, *JHEP* **06** (2014) 097 [arXiv:1401.6364] [INSPIRE].

[25] Z. Nagy and D.E. Soper, *Effects of subleading color in a parton shower*, arXiv:1501.00778 [INSPIRE].

[26] S. Frixione and B.R. Webber, *Matching NLO QCD computations and parton shower simulations*, *JHEP* **06** (2002) 029 [hep-ph/0204244] [INSPIRE].

[27] S. Frixione, P. Nason and B.R. Webber, *Matching NLO QCD and parton showers in heavy flavor production*, *JHEP* **08** (2003) 007 [hep-ph/0305252] [INSPIRE].

[28] P. Nason, *A new method for combining NLO QCD with shower Monte Carlo algorithms*, *JHEP* **11** (2004) 040 [hep-ph/0409146] [INSPIRE].

[29] S. Frixione, P. Nason and C. Oleari, *Matching NLO QCD computations with Parton Shower simulations: the POWHEG method*, *JHEP* **11** (2007) 070 [arXiv:0709.2092] [INSPIRE].

[30] S. Alioli, P. Nason, C. Oleari and E. Re, *A general framework for implementing NLO calculations in shower Monte Carlo programs: the POWHEG BOX*, *JHEP* **06** (2010) 043 [arXiv:1002.2581] [INSPIRE].

[31] C.H. Chung, M. Krämer and T. Robens, *An alternative subtraction scheme for next-to-leading order QCD calculations*, *JHEP* **06** (2011) 144 [arXiv:1012.4948] [INSPIRE].

[32] C.-H. Chung and T. Robens, *Nagy-Soper subtraction scheme for multiparton final states*, *Phys. Rev.* **D 87** (2013) 074032 [arXiv:1209.1569] [INSPIRE].

[33] G. Bevilacqua, M. Czakon, M. Kubocz and M. Worek, *Complete Nagy-Soper subtraction for next-to-leading order calculations in QCD*, *JHEP* **10** (2013) 204 [arXiv:1308.5605] [INSPIRE].

[34] T. Robens, *Nagy-Soper Subtraction: A Review*, *Mod. Phys. Lett.* **A 28** (2013) 1330020 [arXiv:1306.1946] [INSPIRE].

[35] M. Czakon, C.G. Papadopoulos and M. Worek, *Polarizing the Dipoles*, *JHEP* **08** (2009) 085 [arXiv:0905.0883] [INSPIRE].

[36] J.E. Paton and H.-M. Chan, *Generalized veneziano model with isospin*, *Nucl. Phys.* **B 10** (1969) 516 [INSPIRE].

JHEP06(2015)033

[37] F.A. Berends and W. Giele, *The Six Gluon Process as an Example of Weyl-Van Der Waerden Spinor Calculus*, *Nucl. Phys.* **B 294** (1987) 700 [INSPIRE].

[38] F.A. Berends and W.T. Giele, *Recursive Calculations for Processes with n Gluons*, *Nucl. Phys.* **B 306** (1988) 759 [INSPIRE].

[39] M.L. Mangano, S.J. Parke and Z. Xu, *Duality and Multi-Gluon Scattering*, *Nucl. Phys.* **B 298** (1988) 653 [INSPIRE].

[40] M.L. Mangano, *The Color Structure of Gluon Emission*, *Nucl. Phys.* **B 309** (1988) 461 [INSPIRE].

[41] B. Andersson, G. Gustafson, G. Ingelman and T. Sjöstrand, *Parton Fragmentation and String Dynamics*, *Phys. Rept.* **97** (1983) 31 [INSPIRE].

[42] G. Altarelli and G. Parisi, *Asymptotic Freedom in Parton Language*, *Nucl. Phys.* **B 126** (1977) 298 [INSPIRE].

[43] A. Bassetto, M. Ciafaloni and G. Marchesini, *Jet Structure and Infrared Sensitive Quantities in Perturbative QCD*, *Phys. Rept.* **100** (1983) 201 [INSPIRE].

[44] T. Sjöstrand, S. Mrenna and P.Z. Skands, *PYTHIA 6.4 Physics and Manual*, *JHEP* **05** (2006) 026 [hep-ph/0603175] [INSPIRE].

[45] T. Sjöstrand, S. Mrenna and P.Z. Skands, *A Brief Introduction to PYTHIA 8.1*, *Comput. Phys. Commun.* **178** (2008) 852 [arXiv:0710.3820] [INSPIRE].

[46] M. Bähr et al., *HERWIG++ Physics and Manual*, *Eur. Phys. J.* **C 58** (2008) 639 [arXiv:0803.0883] [INSPIRE].

[47] G. Corcella et al., *HERWIG 6: An event generator for hadron emission reactions with interfering gluons (including supersymmetric processes)*, *JHEP* **01** (2001) 010 [hep-ph/0011363] [INSPIRE].

[48] S. Catani, B.R. Webber and G. Marchesini, *QCD coherent branching and semiinclusive processes at large x*, *Nucl. Phys.* **B 349** (1991) 635 [INSPIRE].

[49] M. Krämer, Michael and D.E. Soper, *Next-to-leading order QCD calculations with parton showers. 1. Collinear singularities*, *Phys. Rev.* **D 69** (2004) 054019 [hep-ph/0306222] [INSPIRE].

[50] D.E. Soper, *Next-to-leading order QCD calculations with parton showers. 2. Soft singularities*, *Phys. Rev.* **D 69** (2004) 054020 [hep-ph/0306268] [INSPIRE].

[51] M. Krämer, Michael, S. Mrenna and D.E. Soper, *Next-to-leading order QCD jet production with parton showers and hadronization*, *Phys. Rev.* **D 73** (2006) 014022 [hep-ph/0509127] [INSPIRE].

[52] Z. Nagy and D.E. Soper, *Matching parton showers to NLO computations*, *JHEP* **10** (2005) 024 [hep-ph/0503053] [INSPIRE].

[53] W.T. Giele, D.A. Kosower and P.Z. Skands, *A simple shower and matching algorithm*, *Phys. Rev.* **D 78** (2008) 014026 [arXiv:0707.3652] [INSPIRE].

[54] S. Platzer and S. Gieseke, *Dipole Showers and Automated NLO Matching in HERWIG++*, *Eur. Phys. J.* **C 72** (2012) 2187 [arXiv:1109.6256] [INSPIRE].

[55] P. Torrielli and S. Frixione, *Matching NLO QCD computations with PYTHIA using MC@NLO*, *JHEP* **04** (2010) 110 [arXiv:1002.4293] [INSPIRE].

JHEP06(2015)033

[56] S. Hoche, F. Krauss, M. Schonherr and F. Siegert, *Automating the POWHEG method in Sherpa*, *JHEP* **04** (2011) 024 [arXiv:1008.5399] [INSPIRE].

[57] S. Hoeche, F. Krauss, M. Schonherr and F. Siegert, *A critical appraisal of NLO+PS matching methods*, *JHEP* **09** (2012) 049 [arXiv:1111.1220] [INSPIRE].

[58] R. Frederix et al., *aMC@NLO predictions for Wjj production at the Tevatron*, *JHEP* **02** (2012) 048 [arXiv:1110.5502] [INSPIRE].

[59] J. Alwall et al., *The automated computation of tree-level and next-to-leading order differential cross sections and their matching to parton shower simulations*, *JHEP* **07** (2014) 079 [arXiv:1405.0301] [INSPIRE].

[60] R.S. Thorne, *The effect on PDFs and $\alpha_S(M_Z^2)$ due to changes in flavour scheme and higher twist contributions*, *Eur. Phys. J.* **C 74** (2014) 2958 [arXiv:1402.3536] [INSPIRE].

[61] T. Plehn, D. Rainwater and P.Z. Skands, *Squark and gluino production with jets*, *Phys. Lett.* **B 645** (2007) 217 [hep-ph/0510144] [INSPIRE].

[62] M.L. Mangano, M. Moretti, F. Piccinini and M. Treccani, *Matching matrix elements and shower evolution for top-quark production in hadronic collisions*, *JHEP* **01** (2007) 013 [hep-ph/0611129] [INSPIRE].

[63] S. Alioli, P. Nason, C. Oleari and E. Re, *NLO Higgs boson production via gluon fusion matched with shower in POWHEG*, *JHEP* **04** (2009) 002 [arXiv:0812.0578] [INSPIRE].

[64] S. Hoeche et al., *Next-to-leading order QCD predictions for top-quark pair production with up to two jets merged with a parton shower*, arXiv:1402.6293 [INSPIRE].

[65] G. Bevilacqua et al., *HELAC-NLO*, *Comput. Phys. Commun.* **184** (2013) 986 [arXiv:1110.1499] [INSPIRE].

[66] S. Frixione, Z. Kunszt and A. Signer, *Three jet cross-sections to next-to-leading order*, *Nucl. Phys.* **B 467** (1996) 399 [hep-ph/9512328] [INSPIRE].

[67] Z. Nagy and Z. Trócsányi, *Next-to-leading order calculation of four jet observables in electron positron annihilation*, *Phys. Rev.* **D 59** (1999) 014020 [hep-ph/9806317] [INSPIRE].

[68] Z. Nagy, *Next-to-leading order calculation of three jet observables in hadron hadron collision*, *Phys. Rev.* **D 68** (2003) 094002 [hep-ph/0307268] [INSPIRE].

[69] A. van Hameren, C.G. Papadopoulos and R. Pittau, *Automated one-loop calculations: A proof of concept*, *JHEP* **09** (2009) 106 [arXiv:0903.4665] [INSPIRE].

[70] G. Corcella et al., *HERWIG 6.3 release note*, hep-ph/0107071 [INSPIRE].

[71] J. Alwall et al., *A standard format for Les Houches event files*, *Comput. Phys. Commun.* **176** (2007) 300 [hep-ph/0609017] [INSPIRE].

[72] S. Dittmaier, P. Uwer and S. Weinzierl, *NLO QCD corrections to $t\bar{t}$ + jet production at hadron colliders*, *Phys. Rev. Lett.* **98** (2007) 262002 [hep-ph/0703120] [INSPIRE].

[73] S. Dittmaier, P. Uwer and S. Weinzierl, *Hadronic top-quark pair production in association with a hard jet at next-to-leading order QCD: Phenomenological studies for the Tevatron and the LHC*, *Eur. Phys. J.* **C 59** (2009) 625 [arXiv:0810.0452] [INSPIRE].

[74] K. Melnikov and M. Schulze, *NLO QCD corrections to top quark pair production in association with one hard jet at hadron colliders*, *Nucl. Phys.* **B 840** (2010) 129 [arXiv:1004.3284] [INSPIRE].

JHEP06(2015)033

[75] A. Kardos, C. Papadopoulos and Z. Trócsányi, *Top quark pair production in association with a jet with NLO parton showering*, *Phys. Lett.* **B 705** (2011) 76 [arXiv:1101.2672] [INSPIRE].

[76] S. Alioli, S.-O. Moch and P. Uwer, *Hadronic top-quark pair-production with one jet and parton showering*, *JHEP* **01** (2012) 137 [arXiv:1110.5251] [INSPIRE].

[77] A.D. Martin, W.J. Stirling, R.S. Thorne and G. Watt, *Parton distributions for the LHC*, *Eur. Phys. J.* **C 63** (2009) 189 [arXiv:0901.0002] [INSPIRE].

[78] M. Cacciari, G.P. Salam and G. Soyez, *The anti-k(t) jet clustering algorithm*, *JHEP* **04** (2008) 063 [arXiv:0802.1189] [INSPIRE].

[79] M. Dasgupta and G.P. Salam, *Resummation of the jet broadening in DIS*, *Eur. Phys. J.* **C 24** (2002) 213 [hep-ph/0110213] [INSPIRE].

[80] M. Dasgupta and G.P. Salam, *Resummed event shape variables in DIS*, *JHEP* **08** (2002) 032 [hep-ph/0208073] [INSPIRE].

[81] A. Banfi, G.P. Salam and G. Zanderighi, *Resummed event shapes at hadron - hadron colliders*, *JHEP* **08** (2004) 062 [hep-ph/0407287] [INSPIRE].

[82] G. Bozzi, S. Catani, D. de Florian and M. Grazzini, *Transverse-momentum resummation and the spectrum of the Higgs boson at the LHC*, *Nucl. Phys.* **B 737** (2006) 73 [hep-ph/0508068] [INSPIRE].

[83] G. Bozzi, S. Catani, G. Ferrera, D. de Florian and M. Grazzini, *Production of Drell-Yan lepton pairs in hadron collisions: Transverse-momentum resummation at next-to-next-to-leading logarithmic accuracy*, *Phys. Lett.* **B 696** (2011) 207 [arXiv:1007.2351] [INSPIRE].

[84] S. Hoeche and M. Schonherr, *Uncertainties in next-to-leading order plus parton shower matched simulations of inclusive jet and dijet production*, *Phys. Rev.* **D 86** (2012) 094042 [arXiv:1208.2815] [INSPIRE].

[85] J. Alwall et al., *Comparative study of various algorithms for the merging of parton showers and matrix elements in hadronic collisions*, *Eur. Phys. J.* **C 53** (2008) 473 [arXiv:0706.2569] [INSPIRE].

[86] R. Frederix and S. Frixione, *Merging meets matching in MC@NLO*, *JHEP* **12** (2012) 061 [arXiv:1209.6215] [INSPIRE].

JHEP06(2015)033